SEDIMENT MOVEMENT INDUCED BY SHIPS IN RESTRICTED WATERWAYS

by

Yi-Chung Liou and John B. Herbich

Ocean Engineering Program

August 1976

TAMU-SG-76-209

COE Report No. 188

Partially supported through Institutional Grant 04-5-158-19
to Texas A&M University
by the National Oceanic and Atmospheric
Administration's Office of Sea Grants
Department of Commerce

$4.00

Order from:

Department of Marine Resources Information
Center for Marine Resources
Texas A&M University
College Station, Texas 77843

ABSTRACT

A numerical model using the momentum theory of the propeller and Shields' diagram was developed to study sediment movement induced by a ship's propeller in a restricted waterway. The velocity distribution downstream of the propeller was simulated by the Gaussian normal distribution function. The shear velocity and shear stress were obtained using Sternberg's formulas. Once the ship's speed, depth of the waterway, RPM and diameter of the propeller, and draft of the ship are given, the velocity distribution and the grain size of the initial motion could be obtained from this model. A computer program was developed to solve it. Case studies are presented to show the influence of significant factors on sediment movement at the channel bottom induced by a ship's propeller.

PREFACE

Research described in this report was conducted as part of the research program in the Coastal, Hydraulic and Ocean Engineering Group at Texas A&M University and was partially supported by the NOAA Sea Grant Program at Texas A&M University.

ACKNOWLEDGEMENT

Computer work was partially supported by the Texas Engineering Experiment Station.

The manuscript was edited by Dr. Gisela Mahoney and typed for publication by Ms. Joyce McCabe.

TABLE OF CONTENTS

LIST OF TABLES

LIST OF FIGURES

LIST OF FIGURES - continued

LIST OF SYMBOLS

The following symbols have been used in this paper:

A_o = propeller disc area

a = coefficient

B_o = slot width

b = constant

C = concentration of sediment

C_1 = constant

C_2 = constant

C_T = thrust-loading coefficient

D = diameter of propeller

D_o = diameter of circular orifice

D_s = diameter of grain size

d = grain size

F = force

F_g = gravity force

F_i = inertia force

F_n = supporting force

F_t = frictional force

F_v = viscous force

g = gravitational constant

h = water depth

J_t = speed coefficient

K_T = thrust coefficient

m = mass

n = revolutions per minute

P = probability

p = pressure

Q = discharge

R = vertical distance measured from the axis of the propeller

R_* = Reynolds number of the grain

r = specific gravity of water

γ_s = specific gravity of grain

T = thrust

t = time

U_* = shear velocity

u = velocity in x-direction

$\bar{u}$ = average velocity in x-direction

u' = fluctuating velocity in x-direction

V = longitudinal velocity

V_m = maximum longitudinal velocity

V_o = initial velocity

v = velocity in y-direction

$\bar{v}$ = average velocity in y-direction

v' = fluctuating velocity in y-direction

x = horizontal coordinate

y = vertical coordinate

ρ = density of water

ρ_s = density of grain

ν = kinematic deviation

σ = standard deviation

η = y/x

η_1 = ideal efficiency

τ_c = critical shear stress

τ_o = shear stress

ε_s = diffusion coefficient

CHAPTER I

INTRODUCTION

During a ship's passage, the bottom and sides of the canal section are subjected to jet action induced by the ship's engines. In recent years, more serious consideration has been given specifically to the problem of pollution caused by sediment movement stirred up by the ship's propeller in a restricted waterway. Due to increasing tonnage of crude oil, chemicals, and other commodities over navigation waterways, the maintenance cost of waterways is also increasing. A large portion of the cost is caused by an increase in dredging operations. It has been observed that much of the material that requires maintenance dredging stems from sediment movement induced by ships' propellers. Since sediment movement is a major factor in siltation and subsequently in maintenance dredging, an investigation of the sediment movement induced by a ship passing through a restricted waterway is important to minimize dredging costs and to reduce environmental effects.

A survey of literature revealed a limited amount of published material concerning sediment movement induced by ships in restricted waterways. A numerical model using the momentum theory and Shields' diagram was developed to simulate the prototype. The velocity distribution downstream of the propeller is described by the Gaussian normal distribution function.

The parameters in the Shields diagram include the shear stress and shear velocity and are estimated from Sternberg's formulas (28)*.

---

* Numbers in parentheses refer to references listed on page 83.

Field data from the Corpus Christi channel were used in the case studies presented.

This research may be considered as an initial step in the sediment transport study in the waterway.

Specific objectives of this study can be summarized as:

1) Literature review
2) Development of a computer program for
   (a) calculation of velocity distribution downstream of the propeller,
   (b) determination of the critical grain size for the initial motion, and
3) Use of the proposed procedure in case studies.

CHAPTER II

LITERATURE REVIEW

Sediment Transport

Sediment is transported by flowing water as a bed-load, a saltation load, or as a suspended load. Each mode of transport may occur singly, or combined with one or both remaining modes. Normally, sediment transport occurs intermittently by all three modes.

The bed-load is composed of larger particles that move on or near the bed. This load travels along the bed by rolling or sliding, and is in substantially continuous contact with the bed.

The saltation load consists of material that bounces along the bed. It is moved directly or indirectly by the impact of the bouncing particles. Bagnold visualized the grains in saltation moving like ping-pong balls. It is difficult to distinguish the saltation load from the suspended load.

The suspended load is composed of small particles that are kept in suspension by the upward components of turbulent flow. In regions where clays are eroded, the suspended load is a more important mode of transport compared to the bed-load.

Bed-load Transport Theories and Equations

Although attempts toward a rational approach have been made through the years, the equations to determine bed-load transportation are essentially empirical. Since the turn of the century bed-load has received much attention; yet, bed-load movement still cannot be accurately predicted.

The basic concept assumed that the loose bed material was sliding in layers under the action of flow. Early investigators reasoned that the top layer of the bed is set in motion by shear between the water and the bed. In flows where energy is dissipated primarily to overcome friction, the shear force, τ_o, is called tractive force and is equal to

$$\tau_o = \gamma d S_e$$

in which, γ is the unit weight of the water, d is the depth of flow, and S_e is the slope of the energy gradient. If this shear force becomes larger than the force resisting motion of bed particles the bed will move. Rate of transport is therefore a function of the difference between these two forces. The Du Boys equation for bed-load transportation is the first semi-theoretical approach in which rate of transport is related to the flow conditions. Based on the assumption that a certain quantity of sediment is set in motion by an excessive tractive force, Du Boys (15) concluded that the rate of bed-load transport is proportional to the excess of the prevailing tractive force over the critical value required to initiate movement. Thus, Du Boys proposed the classical bed-load formula:

$$q_s = C_s \tau_o (\tau_o - \tau_c) \qquad (2.2)$$

in which, q_s is the rate of transportation, C_s is a sediment coefficient which depends on the character of the sediment, τ_o and τ_c are the prevailing and critical tractive forces, respectively. The Du Boys equation had been widely used in the past because of its simplicity.

In 1936, Shields (15) developed an equation for bed-load transport. His bed-load equation is dimensionally homogeneous. By considering the

acting forces to be restricted to shear forces, he developed a relation:

$$\frac{\tau_o}{(\gamma_s-\gamma)d_s} = f\left(\frac{U^*d_s}{\nu}\right) \qquad (2.3)$$

where τ_o is the critical shear stress at the bed, γ_s and γ are the specific weights of the sediment and fluid respectively, d_s is the grain size, ν is the kinematic viscosity of the fluid and U^* is the shear velocity. The function f was presented as a shaded area on what has become known as Shields' diagram as shown in Figure 2.1. These data were obtained from flume experiments with fully developed turbulent flows over artificially flattened sediment beds. The value of the critical shear stress was determined by Shields from a graph of observed sediment discharge versus shear stress.

White (32) obtained a relation for flows in which motion around the grain was laminar,

$$\frac{\tau_o}{(\gamma_s-\gamma)d_s} = 0.18 \tan \Theta \qquad (2.4)$$

where Θ is the angle of repose of the sediment immersed in the fluid. The form of the equation was found by considering the interaction of the drag and weight forces on a grain. The numerical constant was determined experimentally. For turbulent flow, White found that the critical shear stress was about one half of that for laminar flow. He attributed the difference to velocity fluctuations in the turbulent flow which cause fluctuation in the boundary shear stress and in the forces acting on the grain.

In 1950, Einstein (13) presented a procedure for computation of

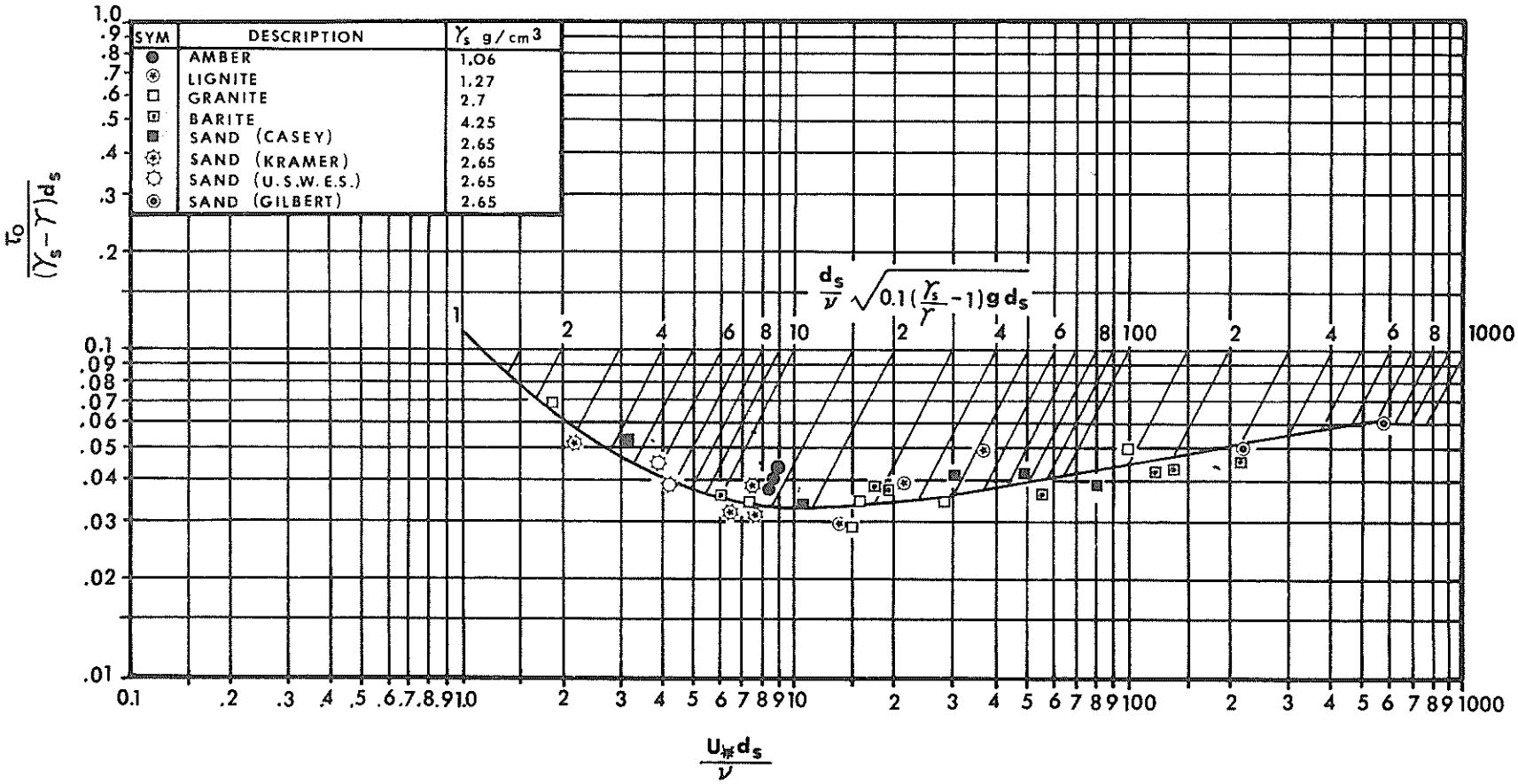

Fig. 2.1- Shields' Diagram for Critical Shear Stress (after ref. 15).

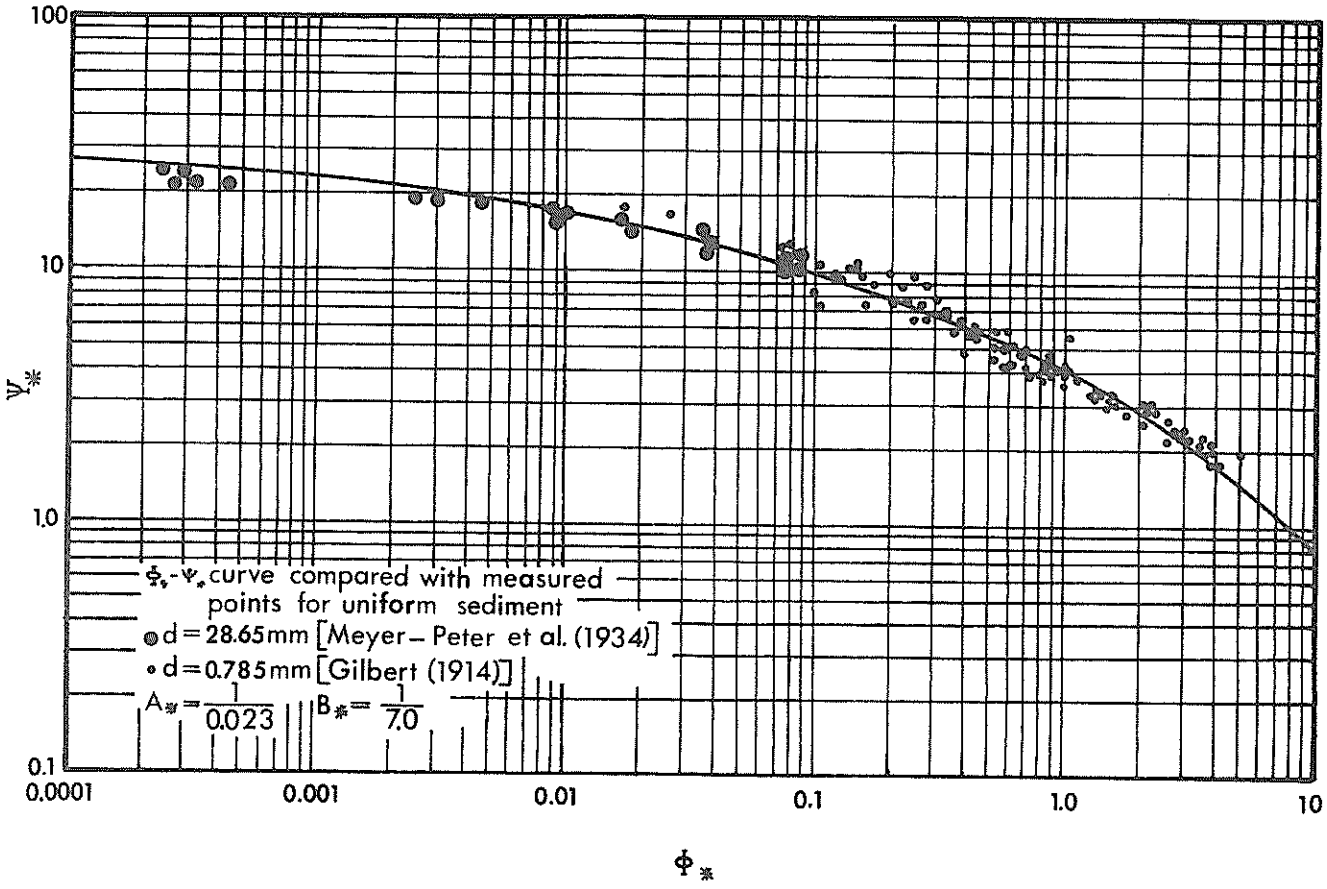

Fig. 2.2- Plot of Einstein Functions ψ^* as a Function of Φ^*.

bed-load discharge from the characteristics of flow and sediment. The Einstein procedure computes the probability of the bed-load movement at the surface as related to intensity of flow. The Einstein bed-load equations may be written

$$P = 1-\frac{1}{\sqrt{\pi}}\int_{-B^*\psi^*-1/\eta_o}^{B^*\psi^*-1/\eta_o} e^{-t^2}\, dt = \frac{A^*\Phi^*}{1-A^*\Phi^*} \tag{2.5}$$

and

$$\Phi^* = \frac{q_B}{\rho_s g}\left(\frac{\rho}{\rho_s-\rho}\right)^{1/2}\left(\frac{1}{gD_s^3}\right)^{1/2} \tag{2.6}$$

where A*, B*, and η_o are universal constants.

If the bed sediment is not uniform in size, the Einstein procedure requires adjustment of Φ and ψ. The adjusted values for individual size classes of bed sediment are Φ^* and ψ^*. The Einstein graph of Φ^* as a function of ψ^* is shown in Fig. 2.2.

The graph shows a rapid decrease of bed-load discharge when ψ^* becomes large. The bed-load discharge of a size fraction is directly proportional to the percentage by weight of that size fraction in the bed sediment for a particular value of Φ^*.

Kalinske (15) applied fluid turbulence concepts to the critical tractive force theory in 1967. He developed a bed-load transport equation as follows:

$$\frac{q_s}{U_*\gamma_s D_s} = f\left(\frac{\tau_c}{\tau_o}\right) \tag{2.7}$$

in which, U_* is the shear velocity, D_s is the grain size, f is a function involving the characteristics of turbulence.

In 1948, the Meyer-Peter formula (11) was developed at the Zurich Hydraulic Laboratory and has been used quite extensively in Europe. It was first published as follows:

$$\frac{q_b^{2/3} S_e}{D_s} = a + b \frac{q_b^{2/3}}{D_s} \tag{2.8}$$

where $q_b = VR_b - V$ is the average velocity of the flow and R_b is the hydraulic radius of the bed.

In 1956, Bagnold (15) developed a theory predicting the relationship between transport function and shear function for materials of uniform grain size. This transport function is composed of (i) a bed-load transport function, ϕ_b, and (ii) a suspended-load transport function, ϕ_s. Assuming the energy distribution is such that the work rate represented by ϕ_s is equal to that represented by ϕ_b, Bagnold derived the functions

$$\phi_s = \phi \left(\frac{B_s}{B_b} \right) \tag{2.9}$$

and

$$\phi_t = \phi_s \left(\frac{1+B_s}{B_b} \right) \tag{2.10}$$

in which ϕ_b, ϕ_s, ϕ_t are the bed-load, suspended load and total transport functions, respectively, and B_b is the dimensionless part of ϕ_b.

In 1972, Sternberg (28) suggested the following formula to estimate the bed-load transport.

$$\left(\frac{\rho_s - \rho}{\rho_s}\right) gj = K\rho U_*^3 \tag{2.11}$$

where j = mass discharge of sediment ($gmcm^{-1}sec^{-1}$); ρ_s = density of

sediment; ρ = fluid density; g = acceleration due to gravity; K is a proportionality coefficient that expresses the ability of a flow to transport sediment; U_* is the friction velocity.

Suspended-load Transport Theories and Equations

If the bed of an alluvial channel contains some percentage of fine particles, then a certain proportion of the transport will be in suspension. Because of the high turbulence level generated by the propeller, the capacity to transport fine grains is high.

In 1933, O'Brien (19) introduced the basic equation for the distribution of suspended material. Assuming the sediment transfer coefficient, ε_s, is approximately equal to the momentum diffusion coefficient, ε_m, he derived the equilibrium equation

$$c\omega = \varepsilon_s \frac{dc}{dy} \tag{2.12}$$

where c is the concentration of sediment at elevation y above the bed, ω is the settling velocity of the sediment and ε_s is a diffusion coefficient for sediment. Integrating the above equation leads to the equation

$$\ln \frac{c}{c_a} = -\omega \int_a^y \frac{dy}{\varepsilon_s} \tag{2.13}$$

in which c_a is the concentration at an arbitrary reference level y = a.

According to Vanoni (31), Von Karman, in 1934, introduced Eq. 2.13 to yield the relationship

$$\ln \frac{c}{c_a} = -\rho\omega \int_a^y \frac{1}{\tau} \left(\frac{d\bar{u}}{dy} \right) dy \tag{2.14}$$

in which, τ is the shear stress. In uniform open-channel flow with a large width to depth ratio the expression for shear at any depth is

$$\tau = \tau_o \frac{d-y}{d} \tag{2.15}$$

in which, τ_o is the shear at the channel bottom and d is the depth of the flow.

Substituting Equation 2.15 into Equation 2.14 yields the relationship

$$\ln \frac{c}{c_a} = - \frac{\omega}{\frac{\tau_o}{\rho}} \int_a^y \frac{\frac{d\bar{u}}{dy}}{\frac{d-y}{d}} \, dy \tag{2.16}$$

Introducing Von Karman's universal velocity defect law

$$\frac{d\bar{u}}{dy} = \frac{1}{k}\sqrt{\frac{\tau_o}{\rho}} \frac{1}{y} \tag{2.17}$$

into Equation 2.16 yields the relationship

$$\ln \frac{c}{c_a} = \frac{\omega}{k\sqrt{\frac{\tau_o}{\rho}}} \int_a^y \frac{1}{y} \frac{dy}{\frac{d-y}{d}} \tag{2.18}$$

in which k is Von Karman's constant. Integrating Equation 2.18 gives the following expression

$$\frac{c}{c_a} = \left(\frac{d-y}{y} \frac{a}{d-a} \right)^z \tag{2.19}$$

where

$$z = \frac{\omega}{k\sqrt{\tau_o/\rho}} \tag{2.20}$$

The suspended load distribution equation was introduced by Rouse in 1937.

Brooks (9) assumed that the velocity distribution is logarithmic, and that concentration follows the suspended load equation:

$$q_s = \int_{y_o}^{d} Cu \, dy \tag{2.21}$$

where

C = concentration of suspended sediment, u = stream velocity, y = distance above the bed, y_o = lower limit of integration, and d = total depth.

The lower limit might reasonably be selected from one of the following equations:

(a) $\eta_o = \frac{2D_s}{d}$

(b) $\eta_o = e^{-k \frac{\bar{u}}{u^*} - 1} \quad u(\eta_o) = 0$

(c) $\eta_o = \left(\frac{C_{md}}{C_b} \right)^{1/z} \quad C(\eta_o) = C_b$

where

$\eta_o = y_{o/d}$

He also suggested that the most reasonable choice would be the equation giving the largest value of η_o.

In 1969, Ammar et al. (4), using Einstein's formula and assuming a logarithmic velocity distribution presented the following:

$$\varphi = \frac{\rho_s - \rho}{\rho} \frac{gD_s}{U_*^2} \tag{2.22}$$

$$u = 5.75 \, U_* \log \frac{y}{y_o} \tag{2.23}$$

where

u = current velocity at a depth y, U_* = shear velocity, $y_o = \frac{D_s}{10}$ for hydraulically rough bed, $\varphi = \frac{D_s}{30}$ for hydraulically smooth bed, and D_s = bed material grain size.

Velocities required to start the motion for particles of specific gravity equal to 2.65 are shown in Table 2.1.

Particle Diameter D(mm)	Water Depth (m)	Incipient Velocity (cm/sec)
0.2	2 3 4 6	33.4 34.4 35.3 36.4
0.06	2 3 4 6	20.2 20.6 21.2 21.8
0.002	2 3 4 6	3.8 3.9 3.96 4.05

Table 2.1- Velocities Required for the Start of Motion (from reference 4)

Garrelts (14), evaluated the influence of the propeller on the bottom of the canal. He showed that the distance separating the circle described by the propeller from the bottom and its thrust-load coefficient are important and influential variables.

Velocity Distribution

As shown by Balanin (7), a jet thrust created by a propeller

can be considered, as a first approximation, at any point of this jet relative to the bank (V_s) as being determined according to the following formula:

$$V_s = \sqrt{\frac{(V_n^2 - V_c^2)\gamma_o^2}{4a^2x^2}\ell - \frac{\gamma^2}{4a^2x^2 + Vc^2 - Vc}} \qquad (2.24)$$

where

V_n = Vo + Vc

V_o = speed in the initial section of a jet (m/sec)

a = coefficient equal to 0.04

γ_o = jet radius in initial section (m)

γ = distance from jet axis to the point where the speed is being sought

x = point coordinate where speed is being sought, in the direction of jet axis

V_c = ship velocity (m/sec)

He also gave the speed in the jet initial section as follows:

$$V_o = \frac{Vc}{2}\left(1 + \sqrt{1 + \frac{2\sigma_{ek}}{\beta}}\right)$$

where

σ_{ek} = engine coefficient of load

β = coefficient 1.14

Approximate computation of the influence on the speed field of a jet thrust-back by an engine of limited surface is done by introduction of an additional, false source located on the opposite side of the limited surface at a distance equal to that of the main source. The unknown value of the speed at any point of jet, allowing for the limited surface, is determined as follows:

$$Vi = \sqrt{V_{i1}^2 + V_{i2}^2} \tag{2.25}$$

For cargo ships the effect of this factor can be neglected since the maximum bottom speed is usually at some distance from the stern and the wake effects are small.

Albertson et al. (3) also state that "since the slip-stream of a propeller differs little from any other type of jet, the velocity distribution in the wake of aircraft and watercraft should be subjected to the same method of analysis".

Rouse (21) showed all of the analytic velocity distribution curves which have been presented for the jet, together with measurements. All the curves are fitted to the measured distributions at point $\bar{u}/\bar{u}_m = 0.5$. He indicated that two curves fit the major portion of the mean velocity distribution very well: the Gaussian distribution and that corresponding to the constant mixing coefficient.

Hilaly (4) gave the following expression for the average return current resulting from a ship passing through the canal:

$$\frac{u}{\sqrt{gh}} = Ko + K_1 \left(\frac{L}{B}\right) + K_2 \left(\frac{P}{T}\right) + K_3 \left(\frac{V}{Vt}\%\right) + K_4 \left(\frac{L}{B}\right)^2 + K_5 \left(\frac{P}{T}\right)^2 \tag{2.26}$$

where

u = the average return current, $Ko = 0.70066$, $K_1 = -0.07219$, $K_2 = -0.5699$, $K_3 = 0.000365$, $K_4 = 0.00608$, $K_5 = 0.17125$, $\frac{L}{B}$ = lateral clearance ratio = mean width of the canal / max ship width, with the mean width of the canal = canal cross-sectional area / canal depth, $\frac{P}{T}$ = vertical clearance ratio = canal depth/ship draft, V = ship's speed, Vt = Schijf's limiting speed, and h = mean canal depth.

CHAPTER III

DEVELOPMENT AND DESCRIPTION OF THE NUMERICAL MODEL

Problem Statement

It was the purpose of this study to develop a numerical model for determining the rate of sediment movement induced by a ship's propeller in a restricted waterway. Figure 3.1 is a definition sketch showing a ship with a propeller of diameter D traveling in a confined waterway of depth h. The propeller turns with a speed usually expressed in revolutions per minute (RPM). When the propeller turns, a turbulent velocity downstream of the propeller will be generated. Since the propeller rotates, both axial and transverse velocity components will be induced.

In order to simplify the problem only the axial velocity in the x-direction, (longitudinal velocity) downstream of the propeller was investigated, and rotational effect of the propeller was neglected. The literature survey indicated no adequate equation to describe this velocity. Thus, a numerical model was used to treat the problem.

The velocity of the propeller's jet can disturb the sediment and cause sediment movement. In order to maintain channel depth, it becomes important to determine the quantity of sediment movement induced by propeller motion in a restricted waterway. The problem involves interaction between the velocity distribution induced by the propeller's jet and the sediment movement caused by this velocity. As the ship passes through the channel, the bottom and sides of the canal section are subjected to jet action due to the ship's propellers. The velocity distribution changes from time to time at a given section. A flat alluvial bed containing different grain sizes will be considered in the

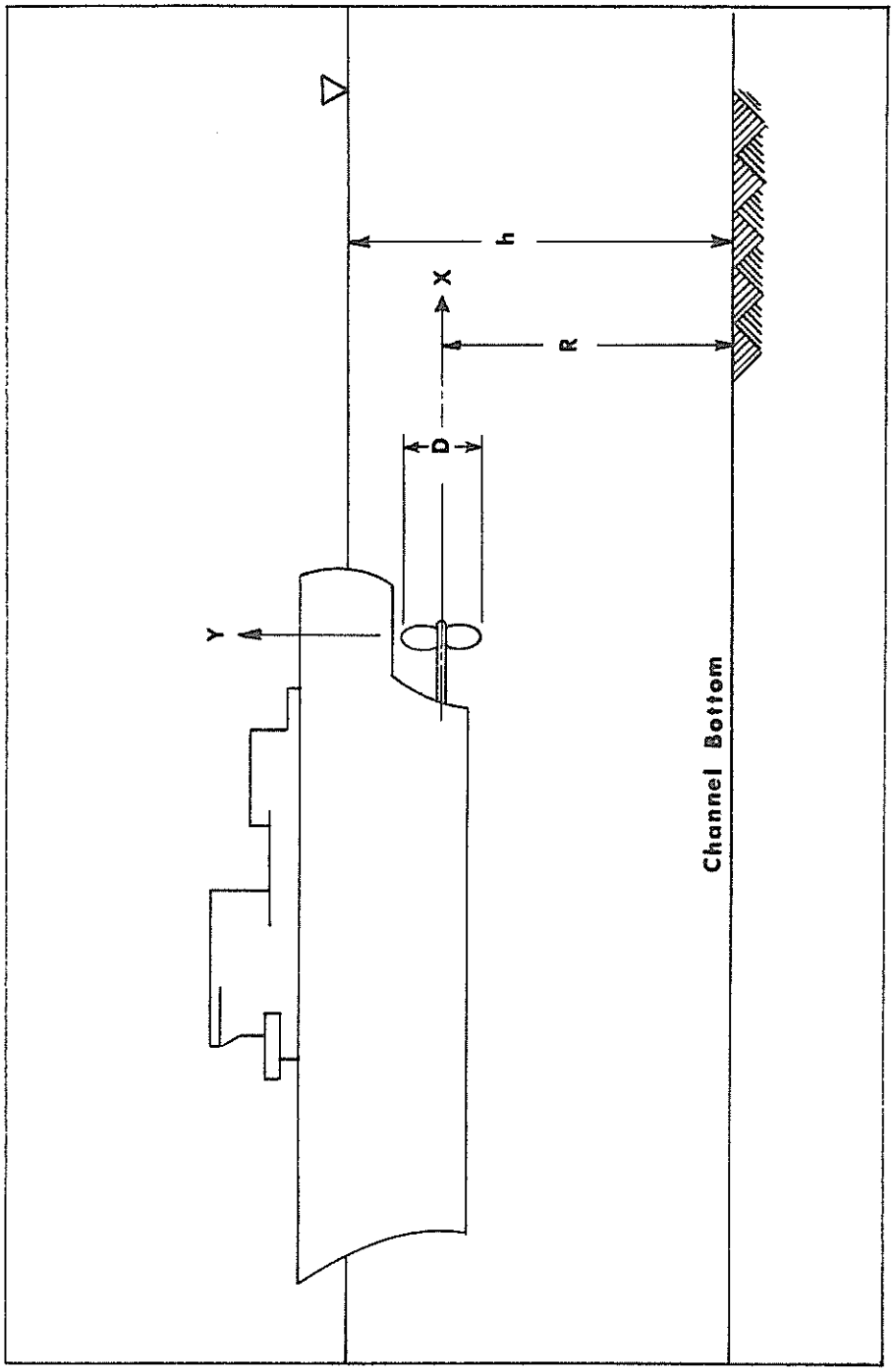

Fig. 3.1 Definition Sketch of a Ship in a Confined Waterway

development of a numerical model. The sediments considered are cohesionless.

Momentum Theory of Propeller Action

Momentum Theory

Propellers derive their propulsive thrust by accelerating the fluid in which they work. This action is in accordance with Newton's law of motion, which states that force is required to alter the existing state of motion of any material body in magnitude or direction, and that the action of any two bodies upon one another is equal and opposite.

Newton's first law is expressed by the equation:

$F = m\, dv/dt$

where F = force exerted on body, m = mass of body, and dv/dt = resulting acceleration of body.

Integrating between 0 and t seconds, we get

$$\int_0^t F\, dt = mv_2 - mv_1 \qquad (3.1)$$

where v_1 and v_2 are the velocities at the beginning and end of the time interval. The expression

$$\int_0^t F\, dt \qquad (3.1a)$$

is called the impulse of the force in the time interval from zero to t, and the product of mass and velocity is called the momentum. The equation states that the impulse of the force in a given time interval is equal to the whole change in momentum produced by the force during this interval.

Momentum Theory of Propeller Action

In the ideal concept, the propeller is regarded as a disk or mechanism capable of imparting a sudden increase of pressure to the fluid passing through it, the method by which it does so being ignored. It is assumed that:

(a) The propeller imparts a uniform acceleration to all the fluid passing through it, so that the thrust thereby generated is uniformly distributed over the disk.

(b) The flow is frictionless.

(c) There is an unlimited inflow of water to the propeller.

Consider a propeller disk of area A_o advancing with uniform velocity V_A into an undisturbed fluid. The hydrodynamic force will be unchanged if we replace this system by a stationary disk in a uniform flow of the same velocity V_A, as shown in Figure 3.2.

At the cross section 1, some distance well ahead of the disk, the velocity of the flow is V_A and the pressure in the fluid is p_1. Well behind the screw, at section 3, the race column, i.e., the fluid which was passed through the screw disk and been acted upon by the pressure or thrust-producing mechanism there, will have some greater sternward velocity, which we may write as $V_A(1 + b)$. The fluid must acquire some of this increased velocity before it reaches the disk, and the velocity through it, at section 2, will be greater than V_A. We may write this velocity as $V_A(1 + a)$, where a is an axial inflow factor.

The pressure in the race column, which is p_1 well ahead of the disk, will be reduced as the fluid approaches the disk, since by Bernoulli's law an increase in velocity is accompanied by a decrease in pressure. At the disk, the pressure is suddenly increased by an

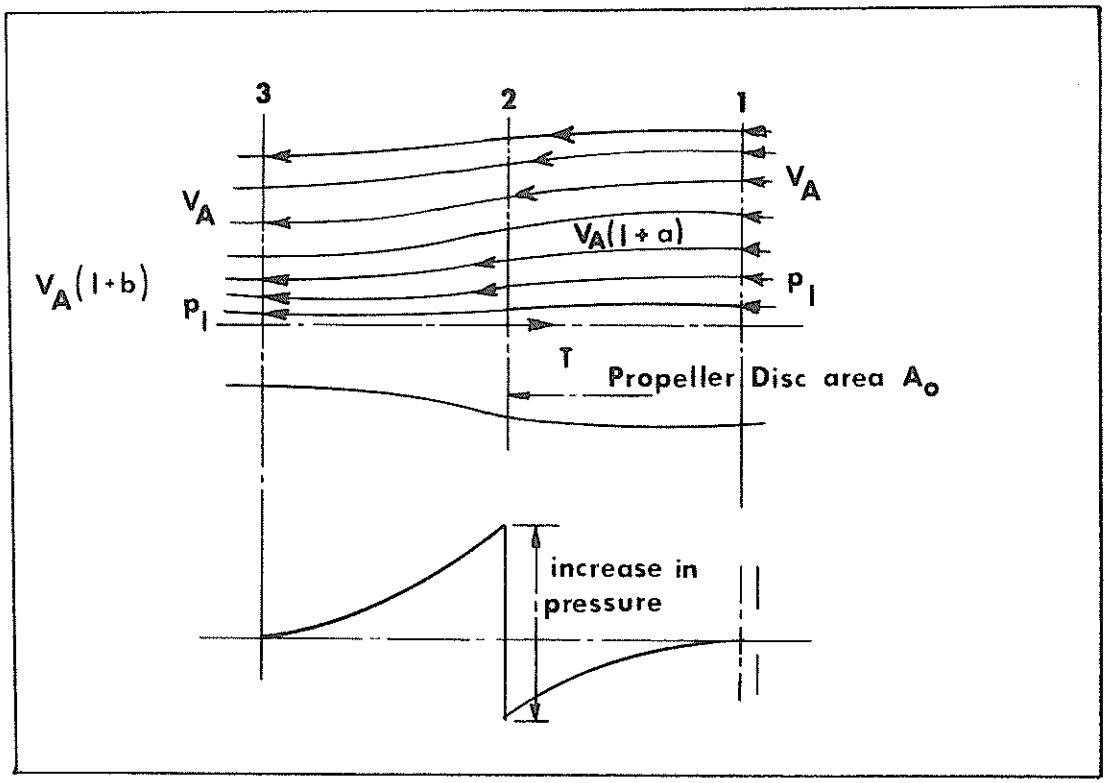

Fig. 3.2 Change in Pressure and Velocity at Propeller Disk, Momentum Theory

unspecific mechanism to some value greater than p_1, and then decreases with further acceleration in the race. If section 3 is so far aft of the disk that the contraction of the race may be assumed to have ceased and, if there is no rotation in the race, the pressure in the race at section 3 will be p_1, equal to that in the fluid outside the race.

The quantity of water passing through the disk in unit time will be

$$Q = V_A(1 + a)A_o \tag{3.2}$$

Neglecting any effect of rotation which may be imparted to the fluid the change of momentum in unit time is

$$\rho Q[V_A(1 + b) - V_A]$$

and this must be equal to the thrust T on the disk.

Hence

$$\begin{aligned} T &= \rho Q V_A b \\ &= \rho A_o (V_A)^2 (1+a) b \end{aligned} \tag{3.3}$$

The total work done per unit time is equal to the increase in kinetic energy of the fluid. Since friction is neglected, and if there is no rotation of the race, the increase in kinetic energy in unit time is given by

$$\begin{aligned} \tfrac{1}{2}\rho Q[(V_A)^2(1 + b)^2 - (V_A)^2] &= \tfrac{1}{2}\rho Q(V_A)^2 b^2 + 2bV_A{}^2) \\ &= \rho Q(V_A)^2 b(1 + \tfrac{b}{2}) \\ &= TV_A(1 + \tfrac{b}{2}) \end{aligned} \tag{3.4}$$

This increase in kinetic energy is provided by the work done on the water by the thrust, which is $TV_A(1 + a)$ in unit time. Hence we have

$$TV_A(1 + a) = TV_A(1 + \frac{b}{2})$$

$$\text{or } a = \frac{b}{2} \tag{3.5}$$

or one half of the sternward increase in velocity is acquired by the fluid before it reaches the disk.

The useful work obtained from the screw, i.e., the work done upon the disk, is TV_A. The ideal efficiency η_1 will be

$$\eta_1 = \frac{\text{useful work obtained}}{\text{work expended}}$$

$$= TV_A/TV_A(1 + a)$$

$$= 1/(1 + a) \tag{3.6}$$

If the thrust-loading coefficient is defined as

$$C_T = \frac{T}{\frac{1}{2}\rho A_o (V_A)^2} \tag{3.7}$$

then

$$\eta_1 = \frac{2}{1 + (C_T + 1)^{1/2}} \tag{3.8}$$

The thrust coefficient (K_T) is given by Comstock (12)

$$K_T = \frac{3600\ T}{\rho n^2 D^4} \tag{3.9}$$

and speed coefficient J_t is given by

$$J_t = \frac{101.33 V_A}{nD} \tag{3.10}$$

where T = thrust, ρ = density of water, n = RPM of propeller, D = diameter of propeller, and V_A = ship speed in knots.

Figure 3.3 shows the propeller's characteristic curve in open water.

To find the average velocity well behind the propeller from the

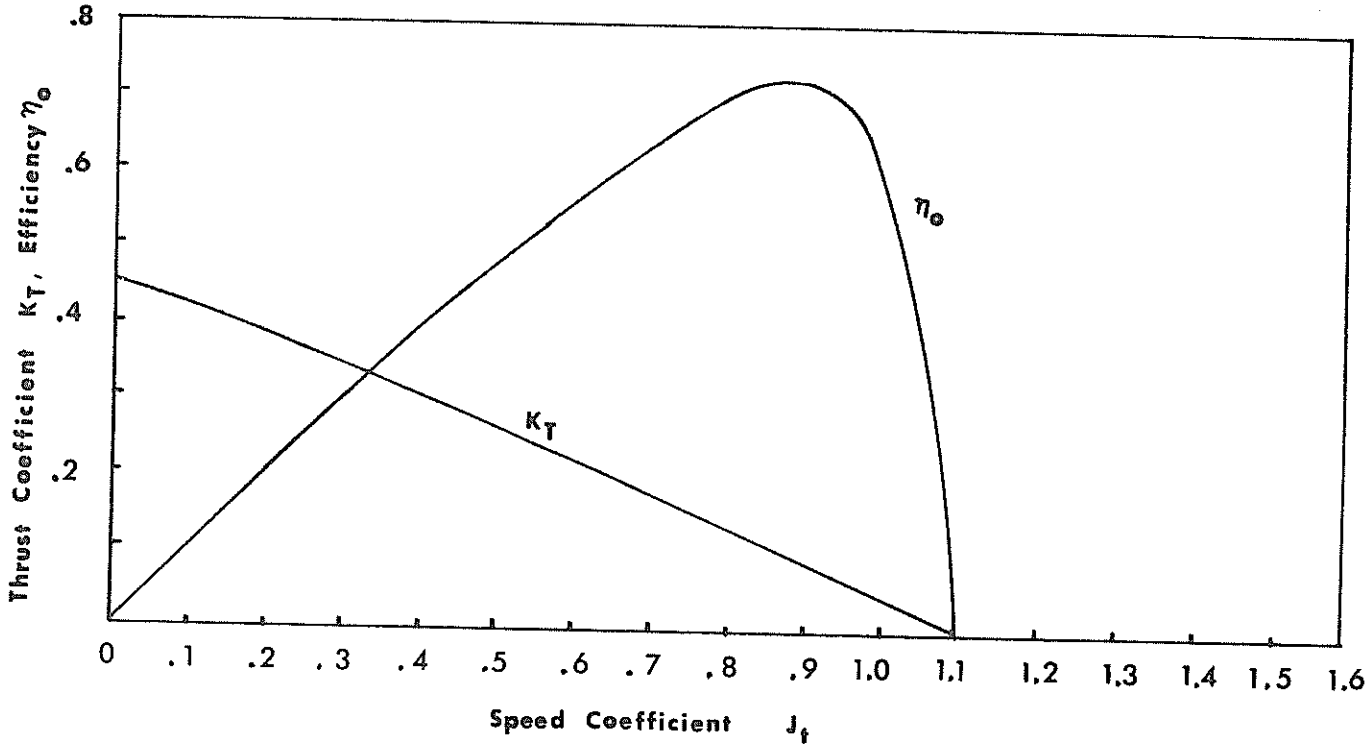

Fig. 3.3 Propeller-Characteristic Curves in Open Water (from Ref. 12)

momentum theory:

1) J_t is obtained from Equation 3.10, the ship's speed, and diameter and speed of the propeller.
2) K_T is obtained from the propeller-characteristic curve.
3) The thrust, T, is evaluated from Equation 3.9.
4) C_T is determined from Equation 3.7.
5) η_1 is obtained from Equation 3.8.
6) Once η_1 is known, and using Equation 3.6, a may be evaluated.
7) b is obtained from Equation 3.5, and then used to solve for $V_A(1 + b)$.

Once the initial velocity downstream of the propeller is known, a numerical model can be developed to simulate the velocity distribution induced by the propeller.

Velocity distribution approach.- The Gaussian normal probability function is used to simulate the velocity distribution downstream of the propeller. It is generally assumed that jets follow the trend of the Gaussian normal probability function (3). In developing a theory of turbulent jets, Albertson, et al. (3) assumed that the pressure distribution was hydrostatic throughout the zone of motion, the momentum flux was constant, and the flow was dynamically similar in every section within the mixing region.

The Gaussian normal probability function can be presented as:

$$\frac{V}{V_m} = \exp\left(\frac{-y^2}{2\sigma^2}\right) \tag{3.11}$$

in which V is the velocity component in the direction of the jet axis, V_m is the axial velocity along the centerline of the jet at any distance

x from the outlet, y is the coordinate normal to x, and where σ mathematically is the standard deviation, and physically is the distance from the centerline of the jet to the point of maximum velocity gradient (Fig. 3.4). There are two zones of flow developed downstream of a jet. As shown in Fig. 3.5, the flow is developed from an initial zone (the zone of flow establishment) to a zone of established flow. The flow establishment zone is just beyond the efflux section. The limit of the zone of flow establishment is reached when the mixing region has penetrated to the central portion of the jet which has become turbulent. The flow may then be considered established. The conditions within the zone of flow establishment and the zone of established flow were first investigated theoretically by Tollmien in 1926. Subsequent studies by other investigators (3) introduced either a concept of vorticity transport or the assumption of constant eddy viscosity across any section of the diffusion zone. No experimental measurements had been made by Tollmien (1).

In 1950, Alberston, et al., (3) used volume flux, momentum flux and energy flux to develop a set of equations for these two different zones. The formulas agreed with experimental measurement and are shown as follows:

Zone of flow establishment

$$\frac{V}{V_o} = \exp\left[-\frac{(y + \frac{1}{2}\sqrt{\pi}C_1x - \frac{1}{2}B_o)^2}{2C_1^2x^2}\right], \qquad (3.12)$$

for

$$y > \frac{B_o}{2} - C_1x,$$

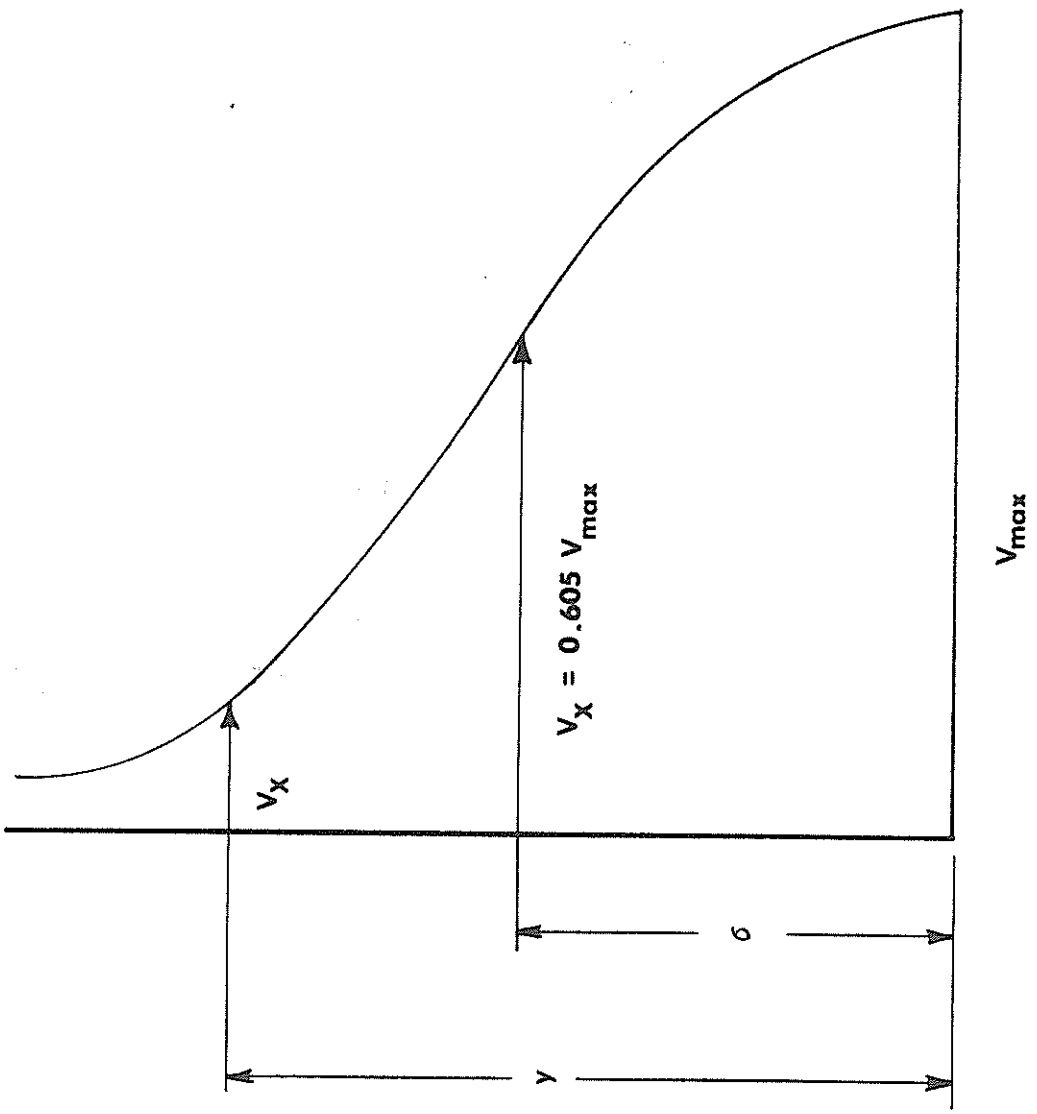

Fig. 3.4 Characteristics of the Normal Probability Curve

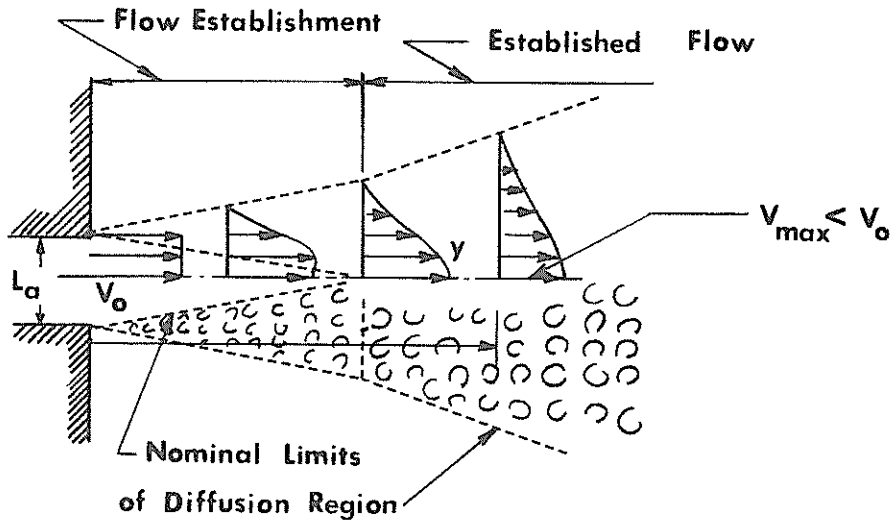

Fig. 3.5 Definition Sketch of Jet Mixing (from Ref. 3)

and $\frac{V}{V_o} = 1$, for $y < \frac{B_o}{2} - C_1 x$, (3.12a)

for the case of a slot,

and

$$\frac{V}{V_o} = \exp\left[\frac{-(r + C_2 x - \frac{1}{2} D_o)^2}{2C_2^2 x^2}\right], \quad (3.13)$$

for

$$y > \frac{D_o}{2} - C_2 x$$

and $\frac{V}{V_o} = 1$, for $y < \frac{D_o}{2} - C_2 x$ (3.13a)

for the case of a circular orifice with r being the radial coordinate. Given the experimentally determined values of C_1 and C_2, the above equations can be expressed as

$$\log_{10} \frac{V}{V_o} = -18.4(0.096 + \frac{y - \frac{1}{2} B_o}{x})^2$$

for the slot, and

$$\log_{10} \frac{V}{V_o} = -33(0.081 + \frac{r - \frac{1}{2} D_o}{x})^2$$

for the circular orifice.

Zone of established flow

$$\frac{V}{V_o} = \sqrt{\frac{1}{C_1 \sqrt{\pi}} \frac{B_o}{x}} \exp\left[-\frac{1}{2C_1^2} \frac{y^2}{x^2}\right] \quad (3.14)$$

for the slot, and

$$\frac{V}{V_o} = \frac{1}{2C_2} \frac{D_o}{x} \exp\left[-\frac{1}{2C_2^2} \frac{r^2}{x^2}\right] \quad (3.15)$$

for the circular orifice.

After substituting the numerical values of C_1 and C_2 into the equations, they can be expressed as

$$\log_{10} \frac{V}{V_o} \sqrt{\frac{x}{B_o}} = 0.36 - 18.4 \frac{y^2}{x^2} \tag{3.14a}$$

for the slot, and

$$\log_{10} \frac{V}{V_o} \frac{x}{D_o} = 0.79 - 33 \frac{r^2}{x^2} \tag{3.15a}$$

for the circular orifice. The equations for the velocity along the center line in the zone of established flow, V_m, can be expressed as

$$\frac{V_m}{V_o} \sqrt{\frac{x}{B_o}} = 2.28 \tag{3.14b}$$

for the slot, and

$$\frac{V_m}{V_o} \frac{x}{D_o} = 6.2 \tag{3.15b}$$

for the circular orifice,

where V = velocity at any point, V_o = initial velocity from jet, D_o = diameter of circular orifice, x = point coordinate where the velocity is being sought, in the direction of jet axis, and C_1, C_2 = constant.

Once the velocity distribution is found, Shields' diagram is used to estimate the initial motion of a particle on the bottom of the channel. Shields' diagram is selected because it is based on experimental data and has been used extensively by other investigators. The parameters in Shields' diagram include the shear stress (τ_o) and the shear velocity (U_*). They can be obtained from Sternberg's (28) formulas:

$$\tau_o = 3 \times 10^{-3} \rho \bar{U}^2_{100} \quad (3.16)$$

$$U_* = 5.47 \times 10^{-2} \bar{U}_{100} \quad (3.17)$$

where ρ = density of water, and $\bar{U}_{100}$ = velocity at one meter above the bottom of the channel.

CHAPTER IV

THEORETICAL STUDIES OF JET AND SEDIMENT MOVEMENT

Theory of Free Turbulence

For the two-dimensional flow of an incompressible fluid, the equation of motion in the x-direction of the boundary layer has the following form:

$$\frac{\partial u}{\partial t} + u\frac{\partial u}{\partial x} + v\frac{\partial u}{\partial y} = \nu\frac{\partial^2 u}{\partial y^2} - \frac{1}{\rho}\frac{\partial p}{\partial x} \tag{4.1}$$

where u and v are the instantaneous values of the velocity components, ρ, p, and ν are the instantaneous values of density, pressure, and kinetic viscosity, respectively.

The equation of continuity for the two-dimensional flow of an incompressible fluid has the form

$$\frac{\partial u}{\partial x} + \frac{\partial v}{\partial y} = 0 \tag{4.2}$$

Multiplying by u, the following equation is obtained:

$$u\frac{\partial u}{\partial x} + u\frac{\partial v}{\partial y} = 0$$

which can also be written in the following form:

$$\frac{\partial (u^2)}{\partial x} + \frac{\partial uv}{\partial y} = u\frac{\partial u}{\partial x} + v\frac{\partial u}{\partial y} \tag{4.3}$$

After substituting equation 4.3 into equation 4.1,

$$\frac{\partial u}{\partial t} + \frac{\partial (u^2)}{\partial x} + \frac{\partial uv}{\partial y} = \nu\frac{\partial^2 u}{\partial y^2} - \frac{1}{\rho}\frac{\partial p}{\partial x} \tag{4.4}$$

The velocity components of turbulent flow and the pressure can be separated into a time average and a fluctuating component

$$u = u + u',\ v = v + v',\ p = p + p' \tag{4.5a}$$

where the time averages of the fluctuating components vanish or

$$v' = 0,\ u' = 0,\ p' = 0. \tag{4.5b}$$

In general, however, this cannot be extended to the square of the fluctuating values and their products. The instantaneous values in equation 4.4 are replaced by the mean and fluctuating values; viscosity and density are assumed constant. Averaging with respect to time, and taking equation 4.5 into consideration we obtain

$$\frac{\partial \bar{u}}{\partial t} + \frac{\partial \bar{u}^2}{\partial x} + \frac{\partial \overline{u'^2}}{\partial x} + \frac{\partial \overline{uv}}{\partial y} + \frac{\partial \overline{u'v'}}{\partial y} = \nu \frac{\partial^2 \bar{u}}{\partial y^2} - \frac{1}{\rho} \frac{\partial \bar{p}}{\partial x} \tag{4.6}$$

The boundary layer of the turbulent flow (Figure 4.1) is assumed to consist of a very thin, laminar sublayer bordering directly on the wall, while the effect of viscosity in the remaining part of the boundary layer is not significant.

A special characteristic of turbulence-free jets is the absence of solid flow boundaries and consequently also of a laminar sublayer, which permits the neglect of the influence of viscosity in all cases of free turbulence. This also explains the self-similarity of jets over a broad range and independent of the Reynolds number.

Free jets expanding into an infinite region filled with a quiescent fluid, and also wakes surrounded by an infinite undisturbed stream, possess such small pressure gradients that in most cases the latter can be neglected.

The equation of motion for the two-dimensional free flow of an incompressible fluid, stationary with respect to mean velocity ($\frac{\partial \bar{u}}{\partial t} = 0$), can be written in the following form:

$$\frac{\partial \bar{u}^2}{\partial x} + \frac{\partial \overline{uv}}{\partial y} + \frac{\partial \overline{u'^2}}{\partial x} + \frac{\partial \overline{u'v'}}{\partial y} = 0 \tag{4.7}$$

or, changing to mean and fluctuating velocities in the equation of continuity [equation 4.2]

$$\frac{\partial \bar{u}}{\partial x} + \frac{\partial \bar{v}}{\partial y} + \frac{\partial u'}{\partial x} + \frac{\partial v'}{\partial y} = 0 \tag{4.8}$$

It follows from equation 4.5 that with a time average the last two terms of this equation vanish, that is, the conventional form of the equation of continuity is valid for the mean velocities:

$$\frac{\partial \bar{u}}{\partial x} + \frac{\partial \bar{v}}{\partial y} = 0 \tag{4.9}$$

Multiplying equation 4.9 by $\bar{u}$,

$$\bar{u} \frac{\partial \bar{u}}{\partial x} + \bar{u} \frac{\partial \bar{v}}{\partial y} = 0 \tag{4.9a}$$

from which follows an equation analogous to equation 4.3:

$$\frac{\partial \bar{u}^2}{\partial x} + \frac{\partial \overline{uv}}{\partial y} = \bar{u} \frac{\partial \bar{u}}{\partial x} + \bar{v} \frac{\partial \bar{u}}{\partial y} \tag{4.9b}$$

Substituting this expression into equation 4.7 leads to the equation for the two-dimensional turbulent boundary layer of a free jet:

$$\bar{u} \frac{\partial \bar{u}}{\partial y} + \nu \frac{\partial \bar{u}}{\partial y} + \frac{\partial \overline{u'^2}}{\partial x} + \frac{\partial \overline{u'v'}}{\partial y} = 0 \tag{4.10}$$

The term $\frac{\partial \overline{u'^2}}{\partial x}$ can be neglected because the velocities and fluctuations of velocity change much more slowly along the flow than in the transverse direction; whereas, the magnitudes of u' and v' are of the same order. Thus

$$u \frac{\partial \bar{u}}{\partial x} + v \frac{\partial \bar{u}}{\partial y} + \frac{\partial \overline{u'v'}}{\partial y} = 0 \tag{4.11}$$

For simplicity, the bars over the mean values of velocity are discarded, that is, u and v signify the time-averaged velocity components.

It is well-known that the equation of motion for the two-dimensional steady isobaric flow of an incompressible fluid can be represented in the following form:

$$u \frac{\partial u}{\partial x} + v \frac{\partial u}{\partial y} = \frac{1}{\rho} \frac{\partial \tau_{xy}}{\partial y} \tag{4.12}$$

where τ_{xy} is the shearing stress acting in a plane perpendicular to the 0_{xy} plane.

Comparing equation 4.12 with equation 4.11 for purely turbulent motion, we arrive at the original relation of the Prandtl theory for the apparent turbulent shearing stress:

$$\tau_{xy} = -\rho \overline{u'v'} \tag{4.13}$$

Prandtl used equation 4.2 and assumed $\ell = cx$ to obtain the equation of two-dimensional motion of Prandtl's old theory of the free turbulence:

$$u \frac{\partial u}{\partial x} + v \frac{\partial u}{\partial y} = \pm 2c^2x^2 \frac{\partial u}{\partial y} \frac{\partial^2 u}{\partial y^2} \tag{4.14}$$

Theory of the Boundary Layer of a Two-Dimensional Turbulent Jet of Incompressible Fluid

As shown in Figure 4.1, a uniform initial velocity field coincides with the boundary of the initial cross section of the jet. The problem of a free-plane boundary layer is solved in coordinates

$$x, \eta = \frac{y}{x}, \text{ and} \tag{4.15}$$

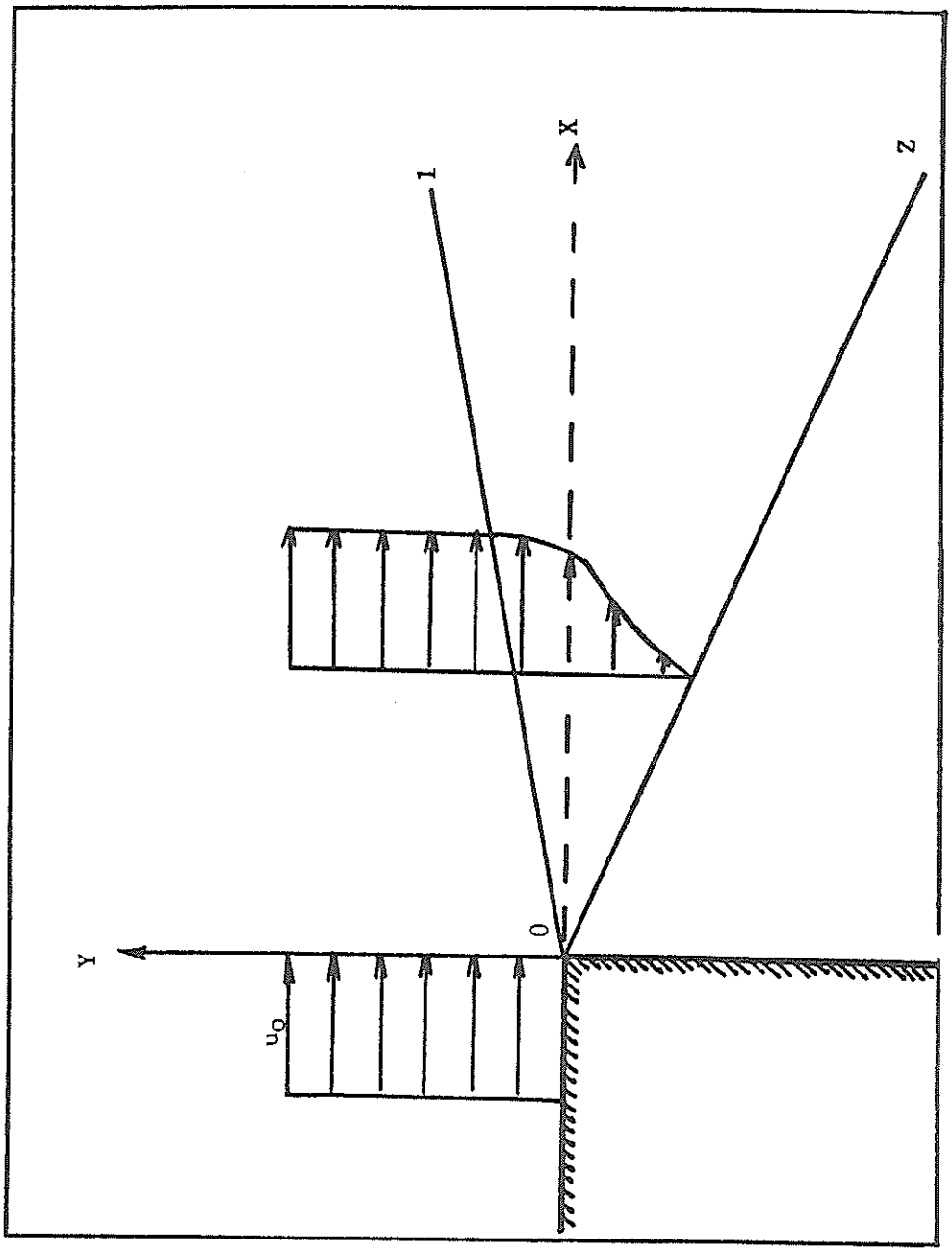

Fig. 4.1 Boundary Layer of a Jet

the velocity depends only on η, or

$$u = u_o f(\eta) \tag{4.16}$$

In order to eliminate the experimental constant from the equation of motion, we assume

$$2c^2 = a^3 \tag{4.17}$$

and we choose the coordinate system

$$x, \quad \psi = \frac{y}{ax} = \frac{\eta}{a} \tag{4.18}$$

where a is an empirical constant characterizing the structure of the flow of a jet. The dimensionless velocity is a function of only one coordinate

$$u = u_o F'(\psi) \tag{4.19}$$

where $F'(\psi)$ is the derivative of a certain function $F(\psi)$, which is proportional to the stream function

$$\int u dy = axu_o \int F' d\psi = axu_o F(\psi) \tag{4.20}$$

By differentiating equation 4.20 the transverse component of velocity can be found:

$$v = -\frac{\partial \psi}{\partial x} = au_o(F' - F) \tag{4.21}$$

Substituting equations 4.19 and 4.21 into equation 4.14, and taking into account

$$a = \sqrt[3]{2c^2},\ \psi = \frac{y}{ax},\ \frac{\partial\psi}{\partial x} = -\frac{\psi}{x},\ \frac{\partial\psi}{\partial y} = \frac{1}{ax}$$

leads to the fundamental equation of the boundary layer of the two-dimensional flow of a jet of an incompressible fluid, when $F'' \neq 0$

$$F''' + F = 0 \tag{4.22}$$

This equation was first obtained by Tollmien (1). The characteristic equation for equation 4.22, $1 + k^3 = 0$, has three roots:

$$k_1 = -1,\ k_2 = -\frac{1}{2} + i\frac{\sqrt{3}}{2},\ k_3 = -\frac{1}{2} - i\frac{\sqrt{3}}{2}$$

The complete integral of equation (4.22) equals

$$F(\psi) = c_1 e^{-\psi} + c_2 e^{\frac{\psi}{2}} \cos\left(\frac{\sqrt{3}}{2}\psi\right) + c_3 e^{\frac{\psi}{2}} \sin\left(\frac{\sqrt{3}}{2}\psi\right) \tag{4.23}$$

The three constants c_1, c_2, c_3 and ordinates ψ_1 and ψ_2 can be evaluated using boundary conditions at the inner and outer edge of the jet.

At the inner edge of the boundary layer ($\psi = \psi_1$)

a) the velocity component along the x-axis (u) equals the upper flow velocity (u_o), that is, according to equation 4.19

$$F'(\psi) = 1 \tag{4.24}$$

b) the velocity component along the y-axis (v) equals zero, that is, according to equation 4.21 and 4.24

$$F(\psi_1) = \psi_1 \tag{4.25}$$

c) the gradient of the horizontal velocity component ($\frac{\partial u}{\partial y}$) equals zero, that is,

$$F''(\psi_1) = 0 \tag{4.26}$$

At the outer edge ($\psi = \psi_2$)

d) the velocity component along the x-axis equals zero, that is

$$F'(\psi_2) = 0 \tag{4.27}$$

e) the gradient of the horizontal velocity component equals zero, that is

$$F''(\psi_2) = 0 \tag{4.28}$$

Using the boundary conditions, we obtain:

$$\psi_1 = 0.981;\ \psi_2 = -2.040$$

$$c_1 = -0.0176;\ c_2 = 0.1337;\ c_3 = 0.6876$$

Substituting these numerical values of the constants into equation (4.23), we obtain the following equation for the desired function:

$$\frac{\psi}{axu_o} = F(\psi) = -0.0176e^{-\psi} + 0.1337e^{\frac{\psi}{2}} \cos\left(\frac{\sqrt{3}}{2}\psi\right) + 0.6876e^{\frac{\psi}{2}} \sin\left(\frac{\sqrt{3}}{2}\psi\right) \tag{4.30}$$

The values of basic and auxiliary functions which allow calculation of dimensionless velocities are given in Table 4.1 (1). In Figure 4.2, Tollmien's velocity profile [equation 4.30] is compared with the experimental data of Albertson, et al. (3) which are taken from Figure 1.9. The value of the empirical coefficient of the structure of the jet is taken to be a = 0.09 and leads to good agreement between theory and experiment.

Table 4.1

Basic Functions of the Boundary Layer of the Jet (from reference (1))

ψ	F	F'	F"	ψ	F	F'	F"
0.98	0.981	1	0	-0.22	-0.021	0.566	0.520
0.93	0.930	0.999	0.048	-0.27	-0.048	0.540	0.519
0.88	0.880	0.995	0.093	-0.32	-0.075	0.514	0.516
0.83	0.831	0.990	0.136	-0.37	-0.100	0.489	0.511
0.78	0.781	0.982	0.176	-0.42	-0.124	0.463	0.506
0.73	0.732	0.972	0.214	-0.47	-0.146	0.438	0.499
0.68	0.684	0.961	0.249	-0.52	-0.167	-.413	0.419
0.63	0.636	0.947	0.282	-0.62	-0.206	-.365	0.472
0.58	0.589	0.932	0.313	-0.72	-0.241	0.319	0.450
0.53	0.543	0.916	0.341	-0.82	-0.270	0.275	0.424
0.48	0.498	0.898	0.367	-0.92	-0.296	0.234	0.396
0.43	0.453	0.871	0.391	-1.02	-0.317	0.196	0.365
0.38	0.410	0.859	0.413	-1.12	-0.335	0.161	0.333
0.33	0.368	0.838	0.432	-1.22	-0.350	0.128	0.300
0.28	0.326	0.816	0.449	-1.32	-0.361	0.101	0.263
0.23	0.286	0.793	0.465	-1.42	-0.370	0.077	0.226
0.18	0.247	0.769	0.478	-1.52	-0.377	0.056	0.189
0.13	0.209	0.745	0.489	-1.62	-0.381	0.039	0.151
0.08	0.172	0.720	0.499	-1.72	-0.384	0.026	0.113
0.03	0.137	0.695	0.507	-1.82	-0.387	0.017	0.074
-0.02	0.103	0.670	0.513	-1.92	-0.388	0.011	0.036
-0.07	0.070	0.644	0.517	-2.02	-0.389	0.009	0
-0.12	0.038	0.618	0.520	-2.04	-0.389	0	0
-0.17	0.008	0.592	0.521				

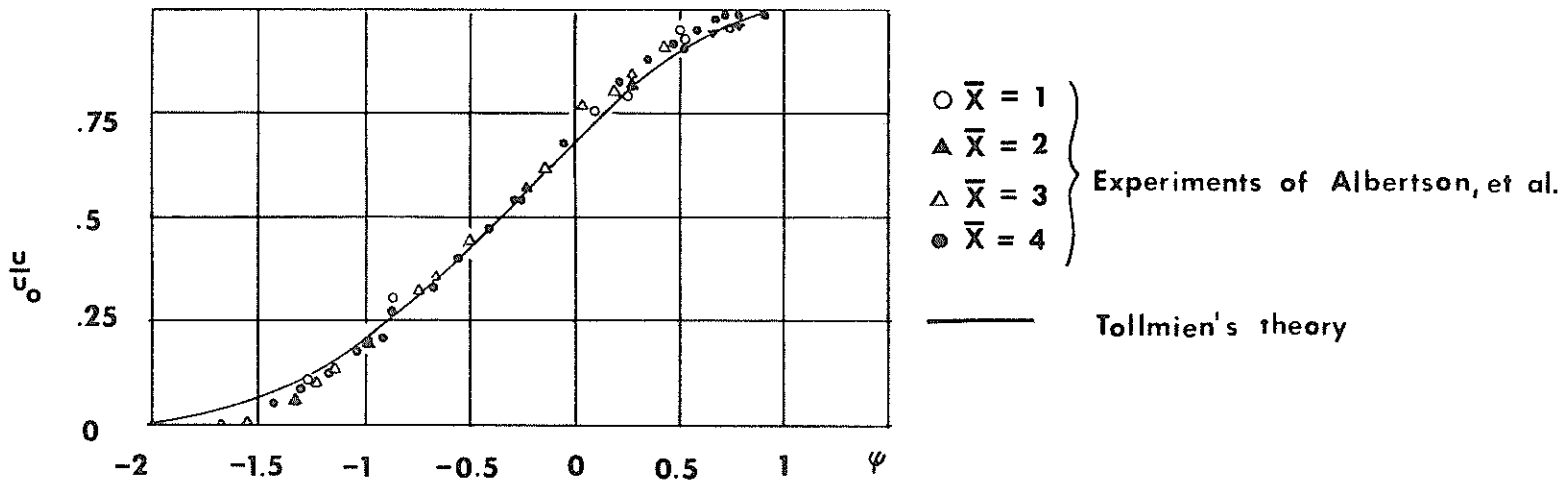

Fig. 4.2 Boundary Velocity Profile of a Submerged Jet
($\bar{x} = x/b_o$)

Theoretical Method for Determining the Rate of Sediment Motion

The bed of an alluvial channel contains coarse and fine sediment. Because of the higher level of turbulence generated by the propeller, the capacity to transport sediment is high. It is very difficult to study sediment motion because of different sizes, angularity, and distribution of sediment in the channel bed.

Similarity Consideration on Incipient Motion

The forces acting upon an individual grain as indicated in Figure 4.3 are gravity force F_g, supporting force F_n, frictional force F_t, and inertia force F_i, acting at the points of contact of the grain with the surrounding grains. Gravity, frictional, and supporting forces resist the motion of the grain, while the inertia and skin friction forces tend to move the grain. The relative magnitudes of these forces determine whether the grain moves or remains stationary. Only the direction of gravity force is well defined. The frictional and supporting forces depend upon the orientation of the supporting grains as well as the shape of the grains. The direction and magnitude of the inertia force is highly affected by the shape of the grain and the arrangement of the particles and the Reynolds number. The viscous force can be disregarded because it is negligible compared to the dominating inertia force. For these conditions only the net gravity and inertia forces need to be considered. If their relative magnitudes reach critical values, the grain will start to move. With F_g proportional to $g(\rho_s-\rho)\ d^3$ and F_i proportional to $\rho u^2 d^2$, the equation is as follows:

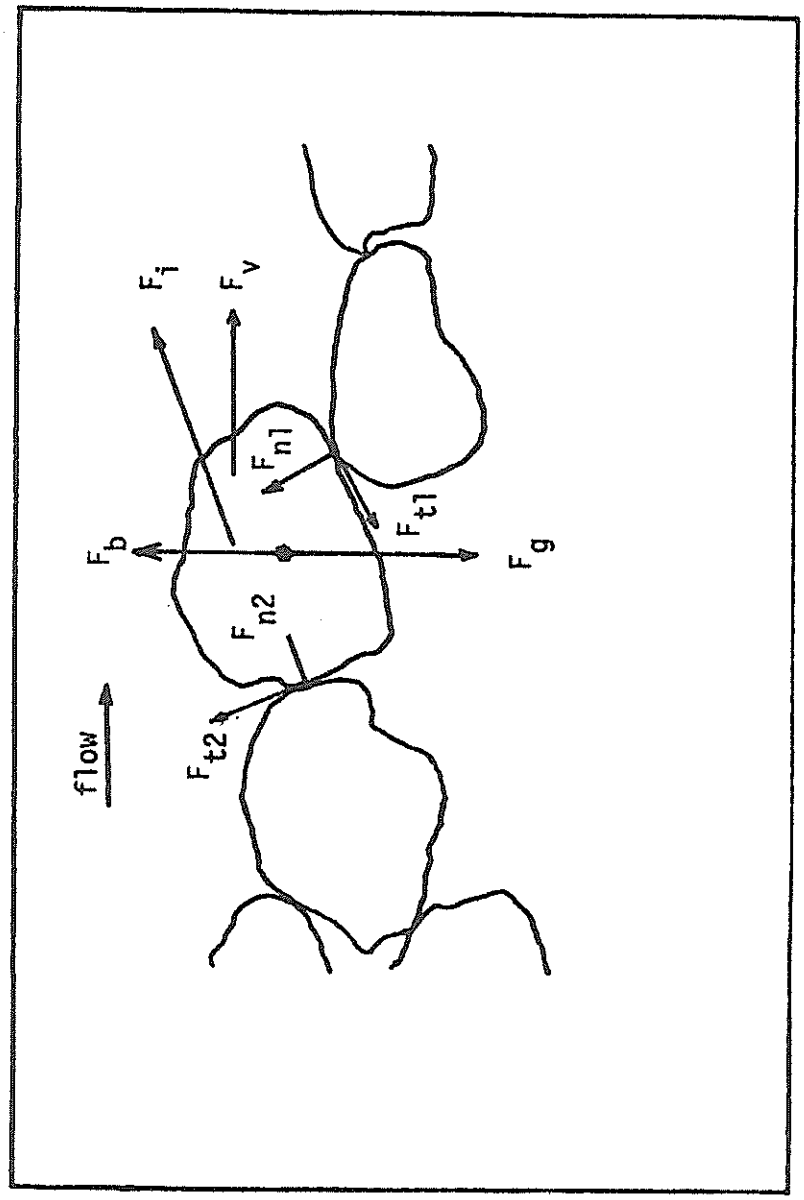

Fig. 4.3 Force Acting on Grain

$$\frac{F_g}{F_i} \alpha \frac{g(\rho_s-\rho)d^3}{\rho u^2 d^2} = \text{constant} \tag{4.31}$$

where u is the local controlling velocity, and it may be selected as the average velocity one grain height above the theoretical boundary. The turbulent-boundary layer theory at a rough wall indicates that these local mean velocities are proportional to the shear velocity, $U_* = \sqrt{\tau_o/\rho}$. Equation 4.31 can be written as

$$\frac{\rho U_*^2}{g(\rho_s-\rho)d} = \frac{\tau_o}{(r_s-r)d} = \text{constant} \tag{4.32}$$

The derivation of equation 4.32 is based on the assumption that the viscous force is much smaller than the form drag, i.e., $F_v < F_i$. If this assumption is not reasonable, the force ratio F_i/F_v should be included.

The viscous shear can be expressed as

$$\tau_v = \mu \frac{du}{dy} \tag{4.33}$$

The velocity gradient, $\frac{du}{dy}$, is the ratio of shear velocity to grain size, U_*/d. For the viscous force

$$F_v = \mu U_* d \tag{4.34}$$

and for the ratio of inertia force over viscous force

$$\frac{F_i}{F_v} \alpha \frac{\rho U_*^2 d}{\mu U_* d} = \frac{U_* d}{\nu} = R_* \tag{4.35}$$

where R_* denotes the Reynolds number of the grain. These two dimensionless parameters are the same as presented by Shields (Figure 2.1).

The Equation of Sediment Continuity

The alteration in the sediment-carrying capacity and the consequent scour or deposition may be expressed in the form of a differential equation. Consider the flow in an alluvial channel of unit width. Let q_s be the volume rate of sediment influx across section AA, and $q + \Delta q_s$ the efflux across section BB, a distance ds further downstream. As a result of the imbalance between the influx and efflux of sediment in the section considered, let there be an erosion $\Delta\eta$ in a time Δt (Fig.4.4). Then we have

$$(q + \Delta q_s)\,\Delta t - q_s \Delta t = \Delta\eta \Delta s \tag{4.36}$$

therefore

$$\Delta q_s \Delta t = \Delta\eta \Delta s \tag{4.37}$$

and hence in the limit

$$\frac{\partial \eta}{\partial t} = \frac{\partial q_s}{\partial s}\,. \tag{4.38}$$

The above equation indicates that the rate of scour in a given section is equal to the gradient of the sediment-carrying capacity in the direction of flow. A solution of this equation for a particular geometry will therefore afford an approximate description of sediment movement.

The sediment-carrying capacity q_s may be expressed in terms of the bed shear, and if the initial flow pattern is known this can be solved for time $t = 0$.

However, the geometry of the bed changes rapidly due to scour and results in a new flow pattern. If an expression can be found for this new flow pattern, a procedure describing the motion may be developed up to the point where there is no further movement of sediment.

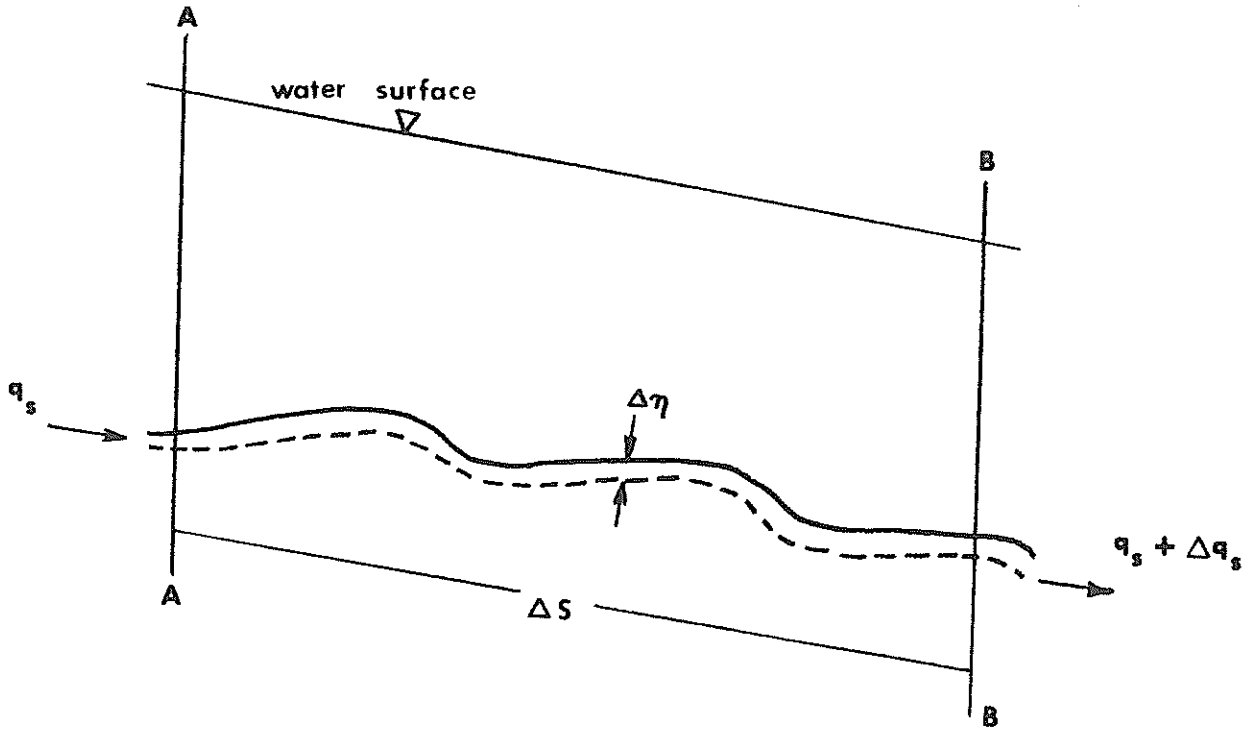

Fig. 4.4 Definition Sketch for Equation of Sediment Continuity

CHAPTER V

PRESENTATION AND DISCUSSION OF RESULTS

Initial Velocity Downstream of the Propeller

As described in Chapter III, the momentum theory of the propeller is used to develop the initial velocity just downstream of the propeller. The procedures are summarized as follows:

1) J_t is obtained from Equation 3.10, the ship's speed, and diameter and speed of the propeller.
2) K_T is obtained from the propeller - characteristic curve.
3) The thrust, T, is evaluated from Equation 3.9.
4) C_T is determined from Equation 3.7.
5) η_1 is obtained from Equation 3.8.
6) Once η_1 is known, and using Equation 3.6, a may be evaluated.
7) b is obtained from Equation 3.5, and then used to solve for $V_A(1 + b)$.

Velocity Distribution

The velocity distribution downstream of the propeller at different positions is simulated by using the formulas for the orifices (Chapter III).

Zone of flow establishment

$$u = u_o \exp\left[- \frac{(r + c_2 x - \frac{1}{2} D_o)^2}{2 c_2^2 x^2} \right] \qquad (3.13)$$

for $r > \frac{D_o}{2} - C_2 x$

and $\frac{u}{u_o} = 1$ for $r < \frac{D_o}{2} - C_2 x$ (3.13a)

Zone of established flow

$$\frac{u}{u_o} = \frac{1}{2C_2} \frac{D_o}{x} \exp\left[-\frac{1}{2C_2^2} \frac{r^2}{x^2}\right] \quad (3.15)$$

Velocity distributions based on these formulas are shown in Figures 5.1 through 5.10, which show the variation of velocity at different locations downstream of the propeller. In Figures 5.1 through 5.10, x is the distance from the propeller, D is the diameter of the propeller, V is the velocity at any point, V_o is the initial velocity well behind the propeller, and R is the distance from the axis of the propeller to the point where the velocity is being sought as shown in Figure 3.1. C_2 is an experimental constant. The value $C_2 = 0.081$ was used in the study.

Initiation of Sediment Movement

Shields' diagram was used to estimate the size of grain which will move. When the shear Reynolds number ($U_* d/\nu$) is greater than 30, a linear function was found between dimensionless critical-shear stress and shear Reynolds number.

$$\left(\frac{\tau_o}{r_s - r}\right) \frac{1}{d} = 0.02 \left(\frac{U_* d}{\nu}\right) 0.183 \quad (5.1)$$

for $R_* = 400$

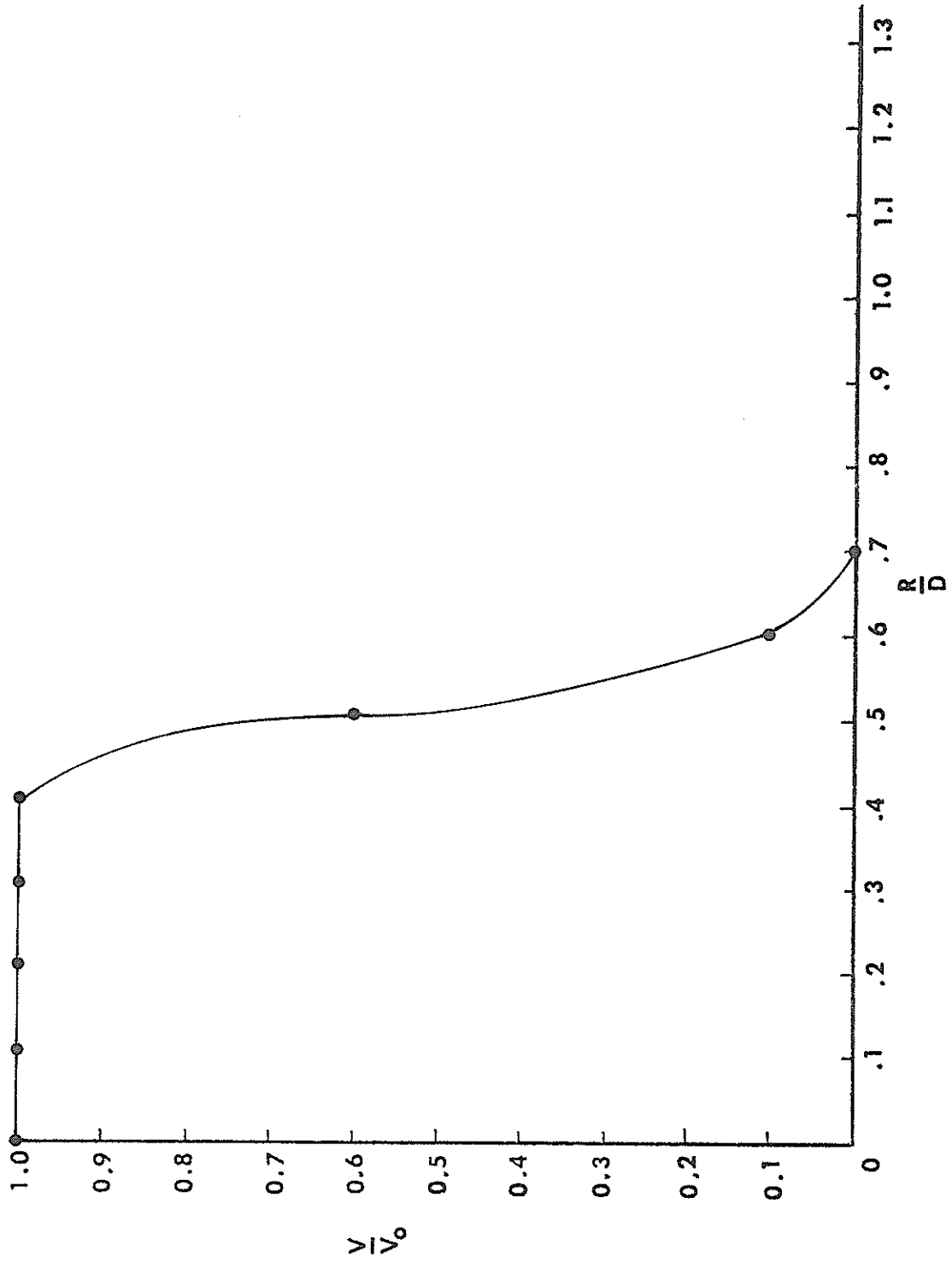

Fig. 5.1 Longitudinal Velocity Distribution at X = D

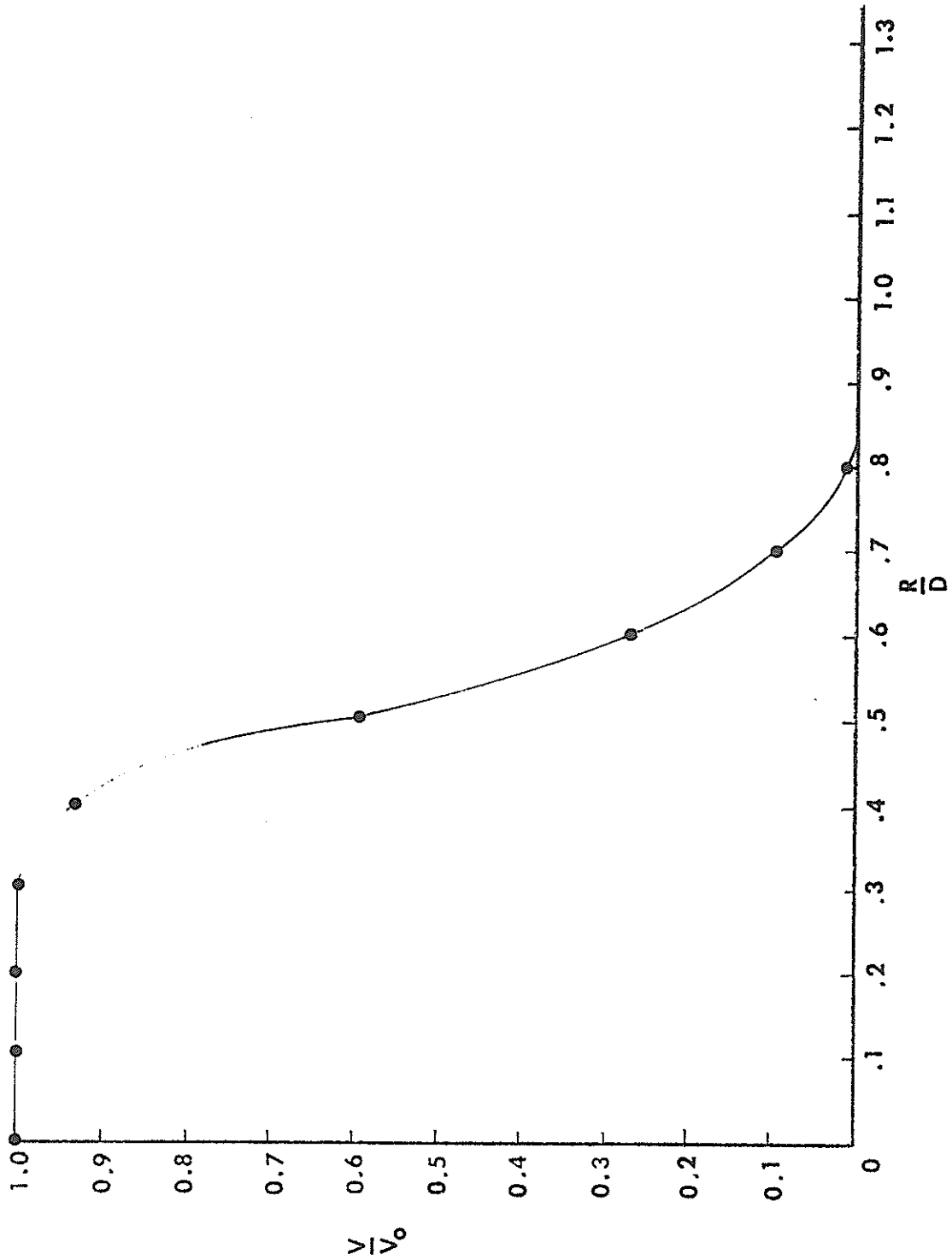

Fig. 5.2 Longitudinal Velocity Distribution at X = 2D

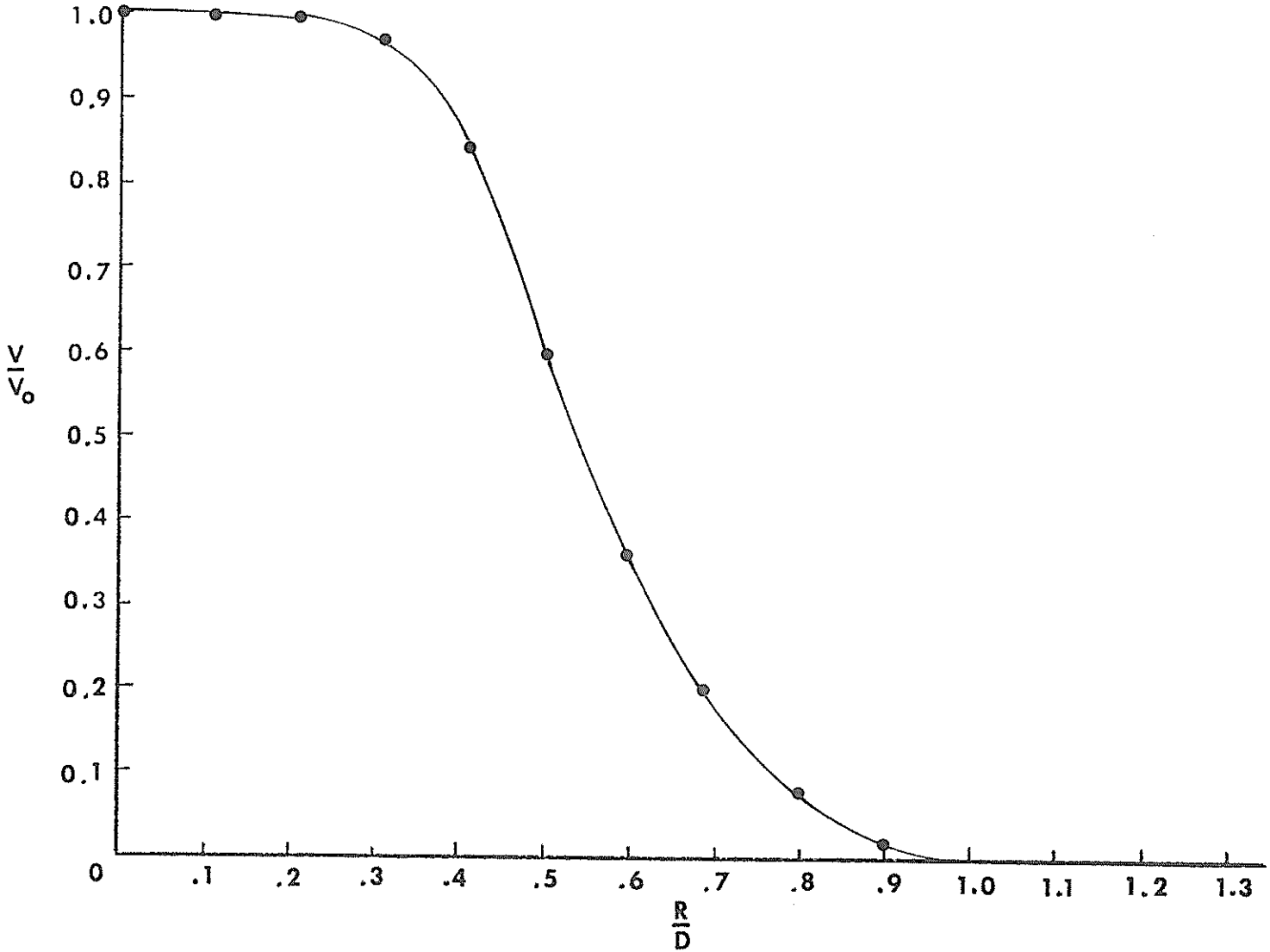

Fig. 5.3 Longitudinal Velocity Distribution at X = 3D

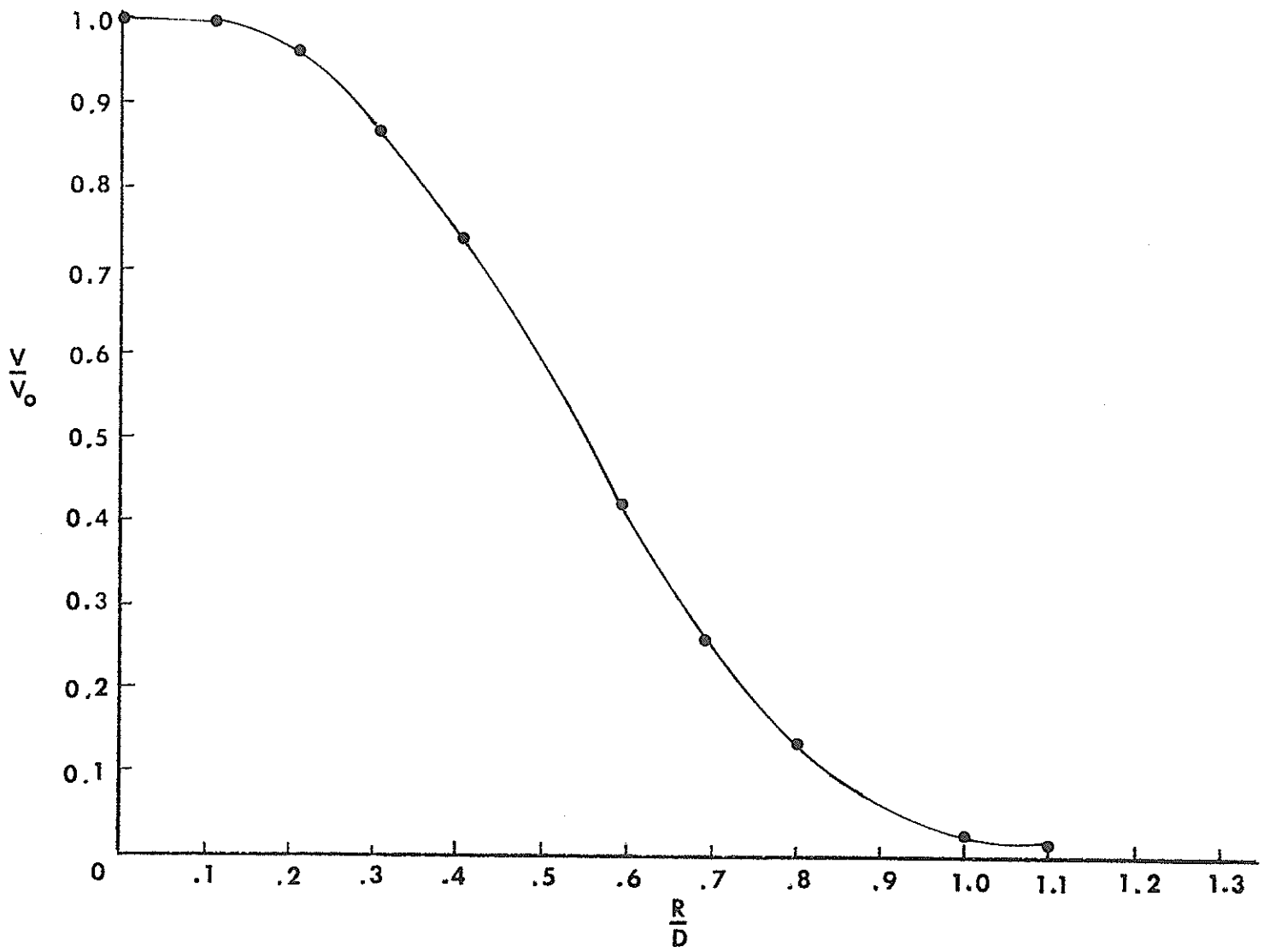

Fig. 5.4 Longitudinal Velocity Distribution at X = 4D

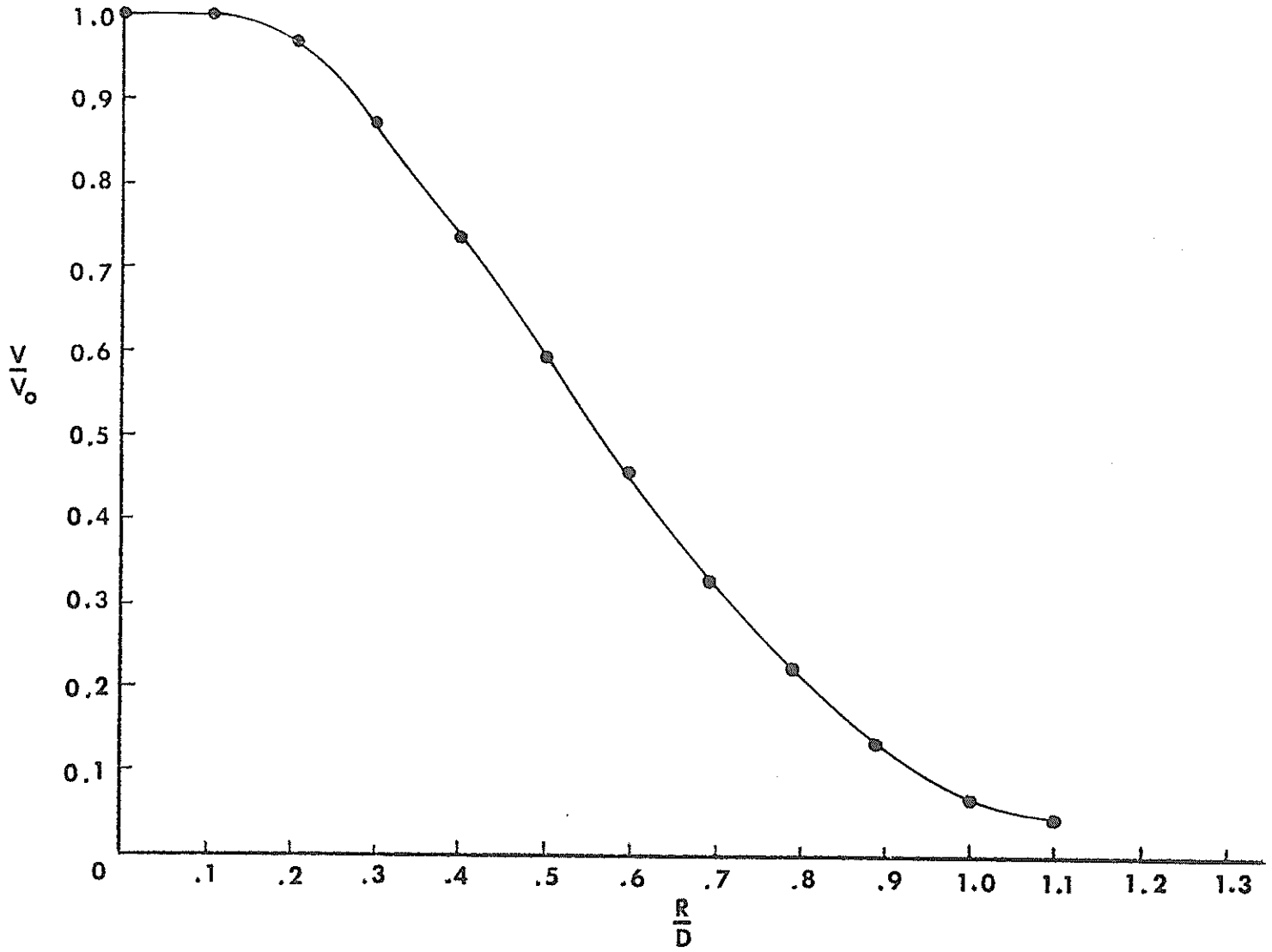

Fig. 5.5 Longitudinal Velocity Distribution at X = 5D

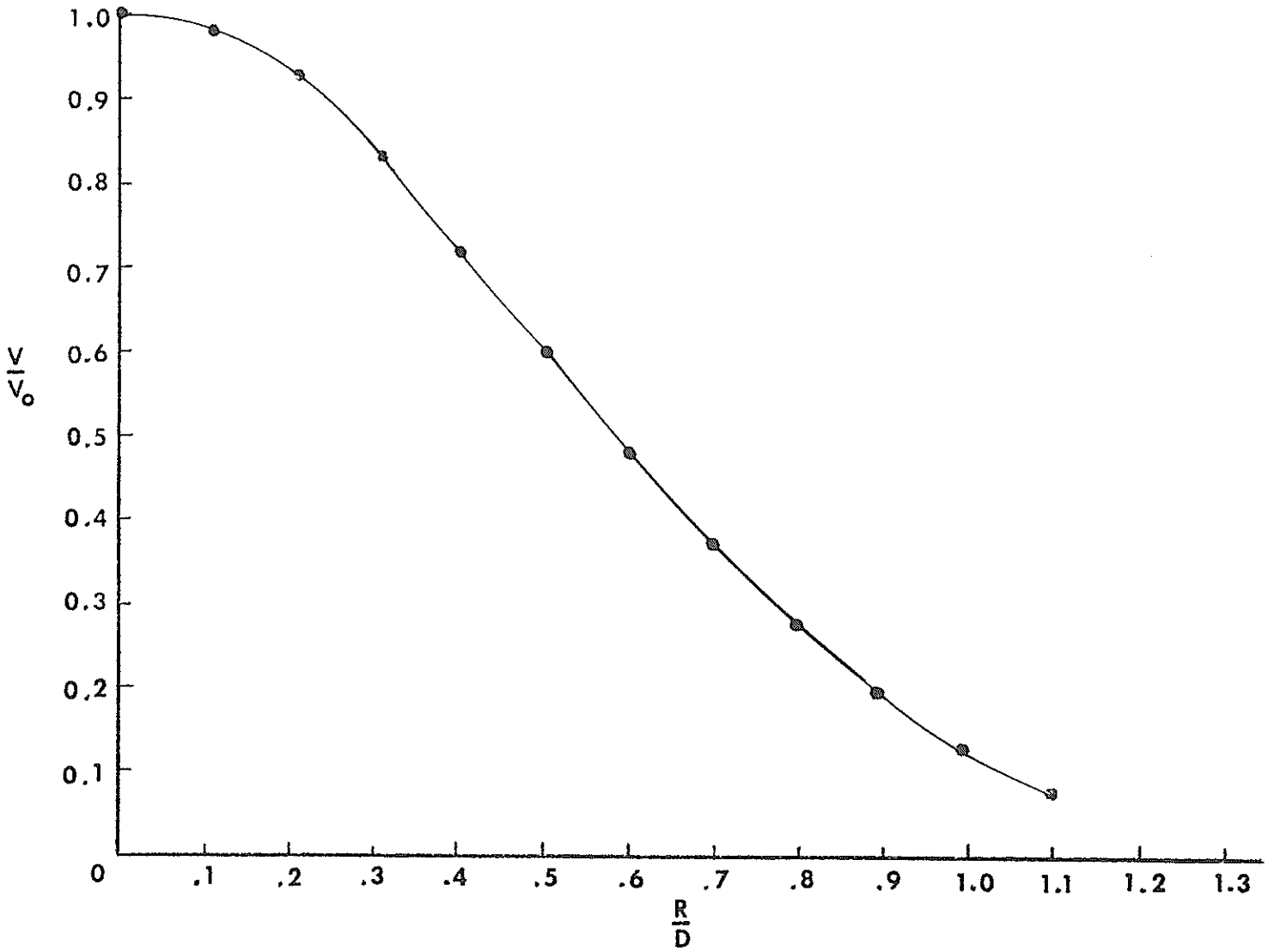

Fig. 5.6 Longitudinal Velocity Distribution at X = 6D

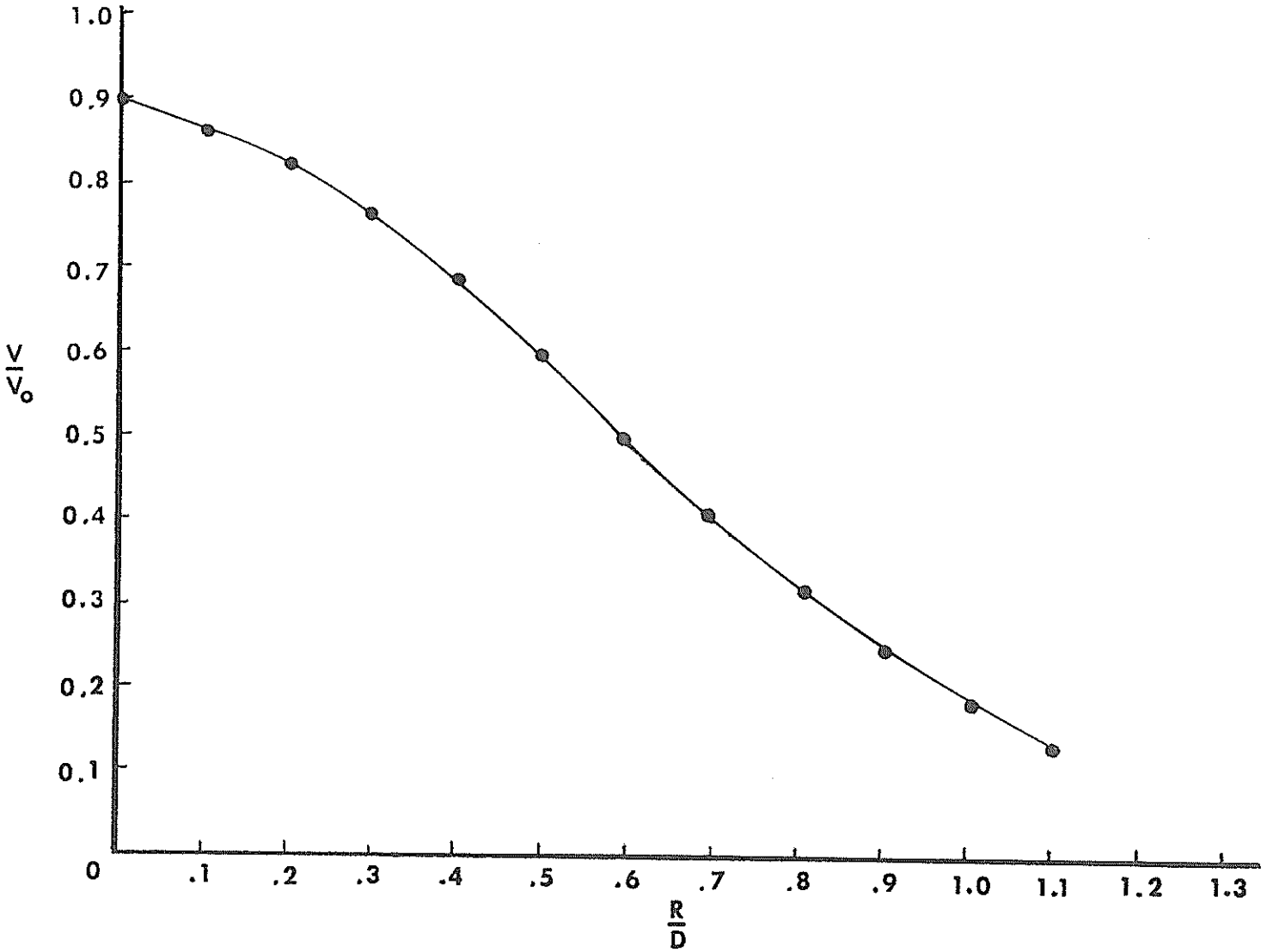

Fig. 5.7 Longitudinal Velocity Distribution at X = 7D

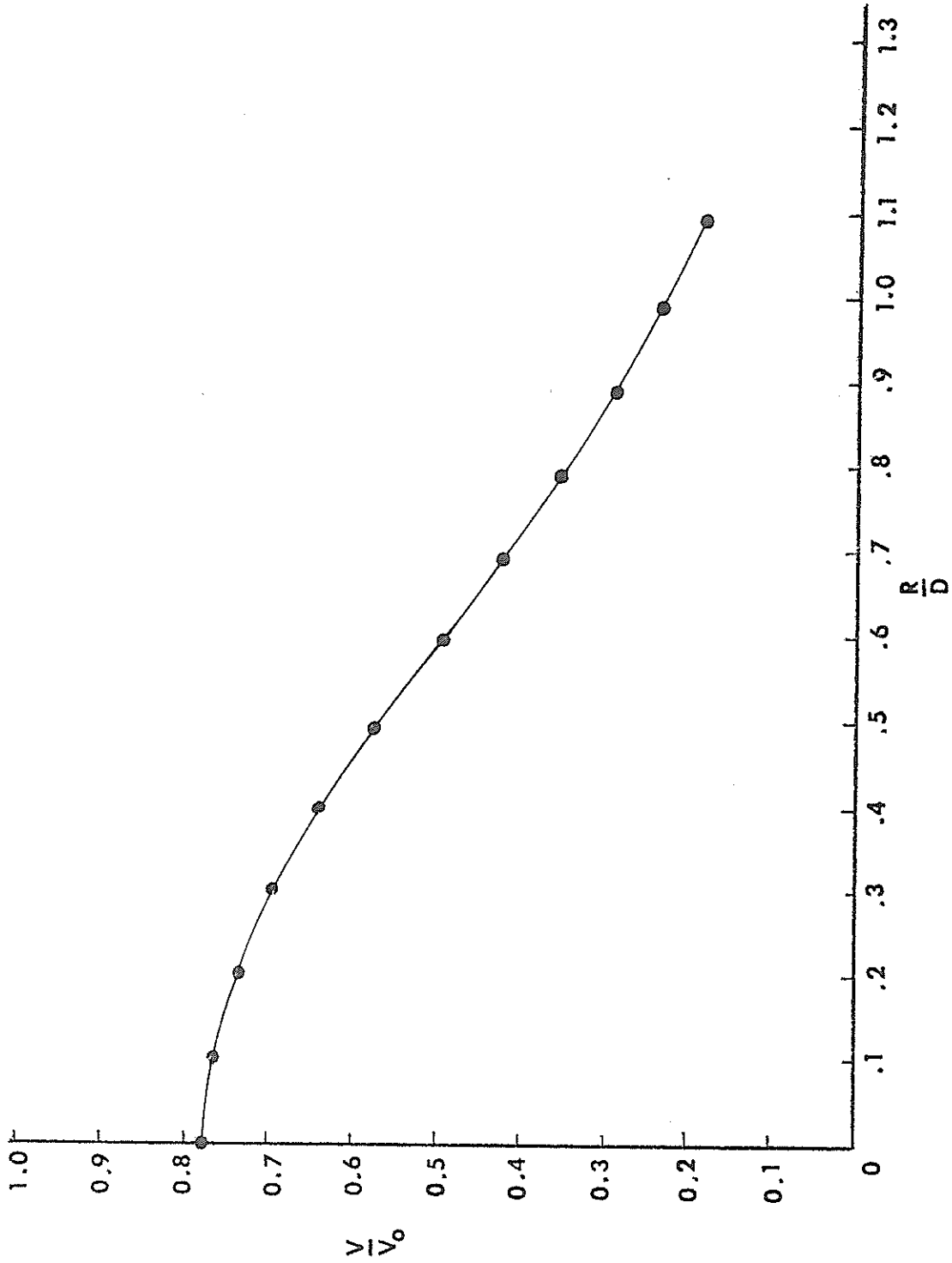

Fig. 5.8 Longitudinal Velocity Distribution at X = 8D

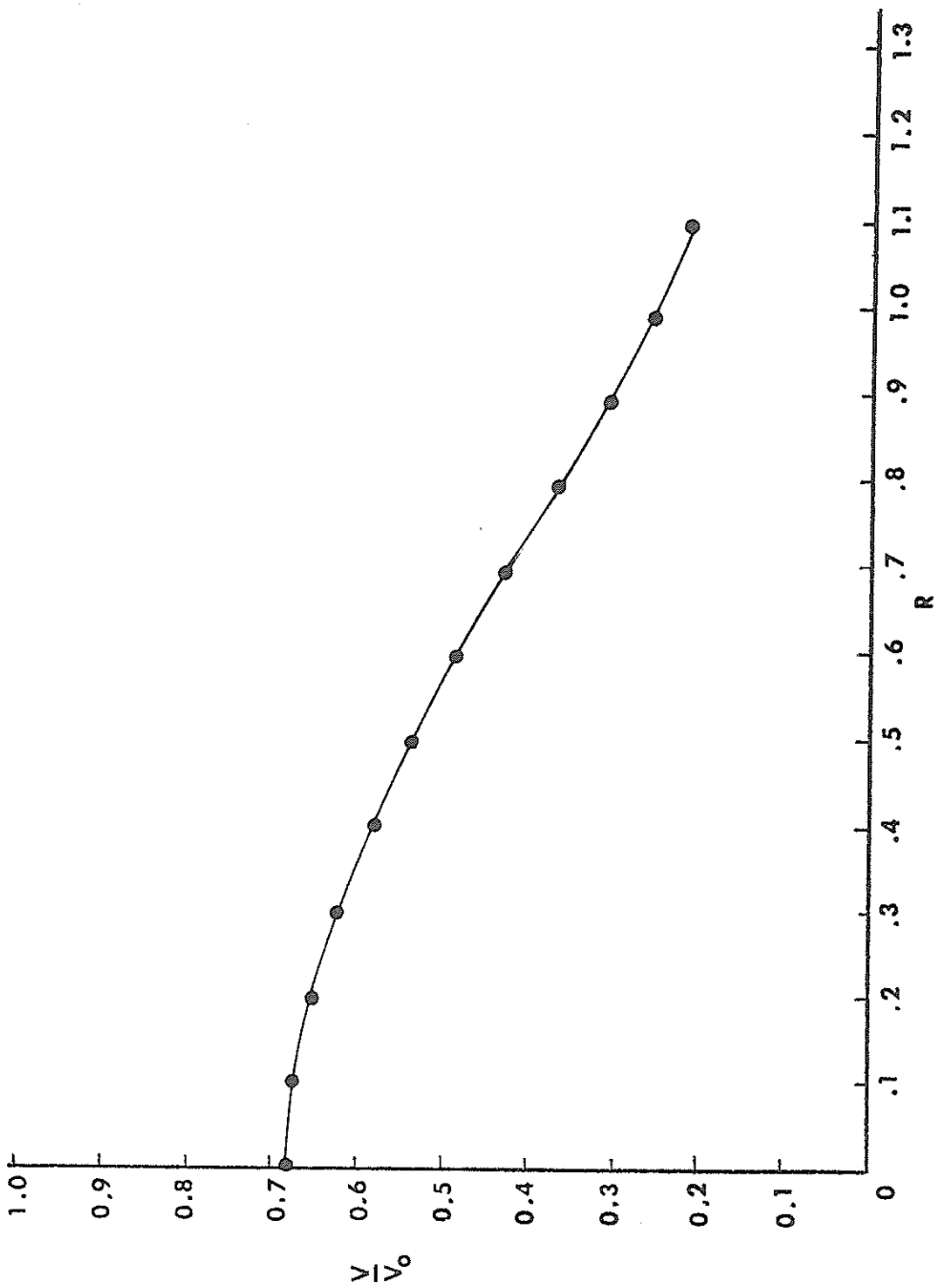

Fig. 5.9 Longitudinal Velocity Distribution at X = 9D

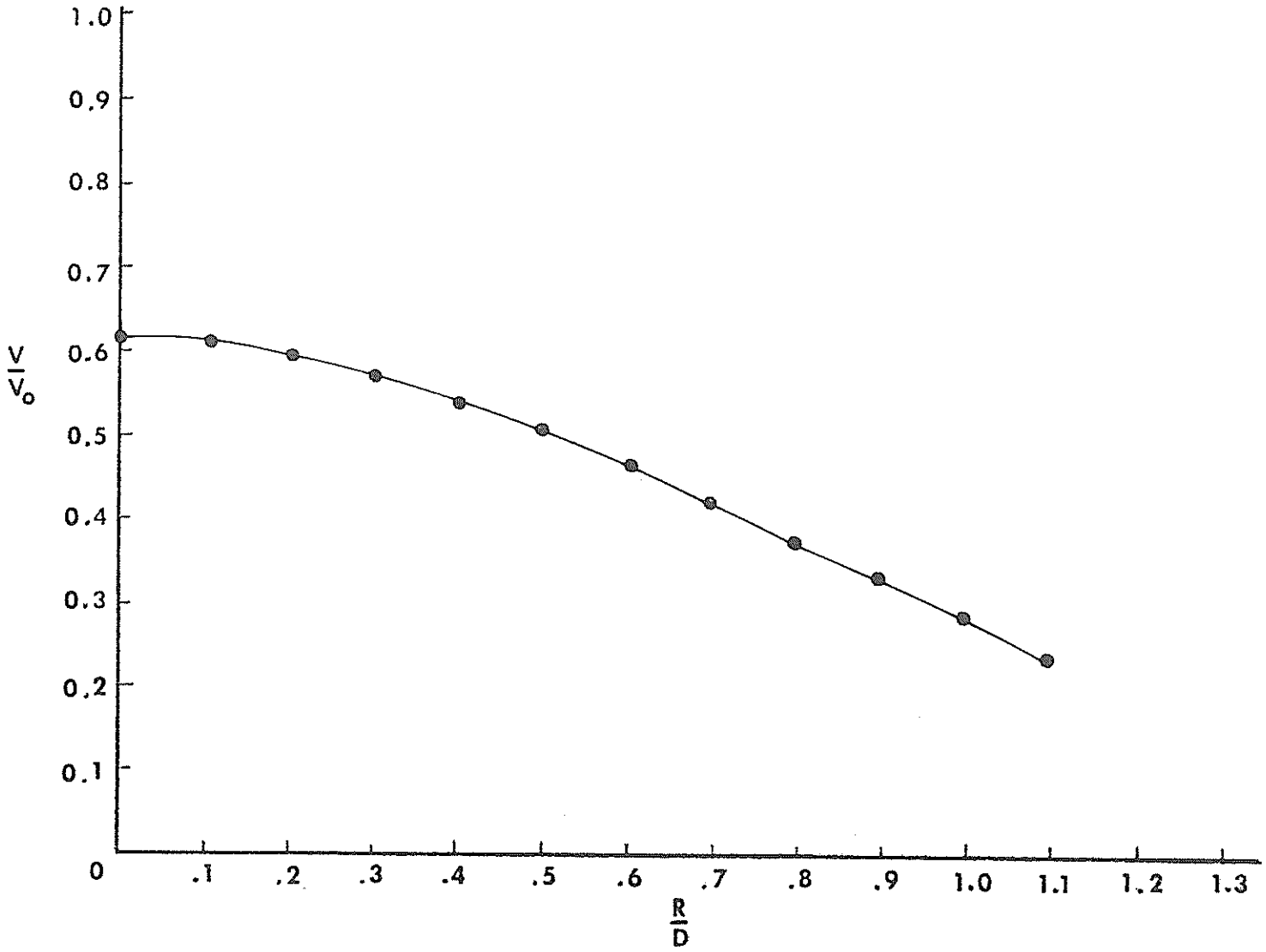

Fig. 5.10 Longitudinal Velocity Distribution at X = 10D

$$\frac{\tau_o}{(r_s - r)} = 0.06 \qquad (5.2)$$

In equations 5.1 and 5.2 shear velocity (U_*) and shear stress (τ_o) can be estimated by using the equations given by Steinberg (28) as shown in Chapter III.

$$\tau_o = 3 \times 10^{-3} \rho \bar{U}_{100}^2 \qquad (3.16)$$

$$U_* = 5.47 \times 10^{-2} \bar{U}_{100} \qquad (3.17)$$

All the steps mentioned previously in this chapter were programmed as shown in Table 5.1 for computer solution. Once the input of the ship's speed, the speed and diameter of the propeller, water depth and draft of the ship are read in this program, the velocity distribution and critical grain size of motion at each location could be obtained. A sample of output for the Tanker TEXAS CALIFORNIA is shown in Table 5.2. Bottom velocities and critical grain sizes from the output are summarized in Table 5.3.

TABLE 5.1 COMPUTER PROGRAM FOR VELOCITY DISTRIBUTION AND CRITICAL GRAIN SIZE OF MOTION

```
C  THIS PROGRAM COMPUTES  VELOCITY DISTRIBUTION AND INITIATION OF SEDIMENT
C  MOVEMENT INDUCED BY SHIP'S PROPELLER IN A RESTRICTED WATERWAY
C  M= NUMBER OF CASE TO BE STUDIED
C  VA= SHIP VELOCITY IN KNOTS
C  N= RPM OF PROPELLER
C  D= DIAMETER OF PROPELLER IN FEET
C  Y= DEPTH OF WATERWAY
C  SD= DRAFT OF SHIP
C  C1= DENSITY OF WATER
C  VO= AVERAGE VELOCITY AFTER PROPELLER
C  GAMS= SPECIFIC GRAVITY OF SAND
C   GAM =  SPFCIFIC GRAVITY OF WATER
C   VI =  VELOCITY  1METER FROM BOTTOM OF THE CHANNEL
C   U = SHEAR VELOCITY U*
C   T =  SHEAR STRESS
C   D50 =  CRITICAL GRAIN SIZE BEGIN TO MOVE
C  BEGIN TO CALCULATE THE AVERAGE VELOCITY AFTER PROPELLER
      READ,M
      C1= 1.99
      C2= 0.081
      GAMS= 2.65
      GAM= 1
      CU= 0.0000121
      DO 400 K=1,M
      READ, VA,N,D,Y,SD
      CJ= 101.33* VA/(N*D)
      CKT = 0.45 - 0.41 *CJ
      T= CKT * C1*N*N*(D**4)/3600
      DT= T/(.5*C1*3.1416/4*D**2*VA**2)
      CT=DT/(1.689**2)
      Z = 1+SQRT(CT+1)
      ETA=2/Z
      B=2/ETA-2
```

TABLE 5.1 (CONTINUED)

```
      VO=VA*(1+B)*1.689
      YO=Y-SD+D/2
      RI= YO-3.3
C END OF CALCULATING AVERAGE VELOCITY AFTER PROPELLER
      XO=D/(2*C2)
      PRINT 150,K
  150 FORMAT('1',T5,'***  CASE',I3)
      DO 20 I=1,10
      X=I*D
      PRINT 100,I
      IF (X.GT.XO) GO TO 10
      DO 30 J=1,21
      R=(J-1)*D/10
      RD=R/D
      IF(R.GT.YO) GO TO 25
      S=D/2-C2*X
      IF(R.LT.S) GO TO 55
      C3=(R+C2*X-D/2)**2
      C4=-C3/(2*(C2*X)**2)
      IF(C4.LT.-20) GO TO 30
      VXI=VO*EXP(C4)
      GO TO 45
   55 VXI=VO
   45 VRI=VXI/VO
      PRINT 200,R,RD,VXI,VRI
   30 CONTINUE
   25 PRINT 80
   80 FORMAT('0','***** VELOCITY IN REGION I ******')
      IF( RI.LT.0) GO TO 20
      C7= (RI+C2*X-D/2) **2
      C8= -C7/(2*(C2*X)**2)
      IF(C8.LT.-20) GO TO 20
      VI= VO* EXP(C8)
```

TABLE 5.1 (CONTINUED)

```
      GO TO 50
C VELOCITY IN REGION II
   10 DO 40 J=1,31
      R=(J-1)*D/10
      RD=R/D
      IF(R.GT.YO) GO TO 35
      C5= -1/(2*C2**2)*(R/X)**2
      C6=(1/(2*C2)*D/X)*EXP(C5)
      VXII= VO*C6
      VRII=VXII/VO
      PRINT 200,R,RD,VXII,VRII
   40 CONTINUE
   35 PRINT 50
   60 FORMAT('0',' ***** VELOCITY IN REGION II *****')
      IF( RI.LT.0) GO TO 20
      C9= -1/(2*C2**2)*(RI/X)**2
      C10= (1/(2*C2)*D/X)*EXP(C9)
      VI= VO* C10
   50 U= 5.47*0.01*VI
      T=3*0.001*C1*(VI**2)
      B1= T/(GAMS-GAM)
      B2=(U/CU)**0.183
      B3= 1/B2
      B4=B1*B3*50
      B5=ALOG(B4)
      B6=B5/1.183
      D50= EXP(B6)
      RE=U*D50/CU
      IF(RE.GT.400) GO TO 51
      GO TO 52
   51 D50=T/(0.06*(GAMS-GAM))
   52 PRINT 250
```

TABLE 5.1 (CONTINUED)

```
250 FORMAT('0',T3,'BOTTOM VELOCITY',T20,'SHEAR STRESS',T40,'SHEAR VELO
   1CITY',T60,'GRAIN SIZE')
    PRINT 300,VI,T,U,D50
300 FORMAT('0',T5,E11.3,T21,E10.3,T42,E10.3,T62,E10.3)
100 FORMAT('0',T25,'X/D=',I3,3(/),T10,'R',T20,'R/D',T30,'LONGITUDINAL
   2 VELOCITY',T60,'V/VO')
200 FORMAT(' ',T7,F5.1,T20,F5.1,T35,F10.5,T60,F5.3)
 20 CONTINUE
400 CONTINUE
    STOP
    END
```

TABLE 5.2 COMPUTER OUTPUT FOR THE "TEXAS CALIFORNIA"

X/D= 1

R	R/D	LONGITUDINAL VELOCITY (ft/sec)	V/VO
0.0	0.0	42.09247	1.000
2.4	0.1	42.09247	1.000
4.8	0.2	42.09247	1.000
7.3	0.3	42.09247	1.000
9.7	0.4	42.09247	1.000
12.1	0.5	25.53036	0.607
14.5	0.6	3.46677	0.082
16.9	0.7	0.10253	0.002
19.4	0.8	0.00066	0.000

***** VELOCITY IN REGION I ******

BOTTOM VELOCITY	SHEAR STRESS	SHEAR VELOCITY (ft/sec)	GRAIN SIZE (ft/sec)
0.218E 00	0.283E-03	0.119E-01	0.617E-02

X/D= 2

R	R/D	LONGITUDINAL VELOCITY	V/VO
0.0	0.0	42.09247	1.000
2.4	0.1	42.09247	1.000
4.8	0.2	42.09247	1.000
7.3	0.3	42.09247	1.000
9.7	0.4	39.11996	0.929
12.1	0.5	25.53043	0.607
14.5	0.6	11.38241	0.270
16.9	0.7	3.46679	0.082
19.4	0.8	0.72133	0.017

TABLE 5.2 (CONTINUED)

***** VELOCITY IN REGION I ******

BOTTOM VELOCITY	SHEAR STRESS	SHEAR VELOCITY	GRAIN SIZE
0.443E 01	0.117E 00	0.242E 00	0.118E 01

X/D= 3

R	R/D	LONGITUDINAL VELOCITY	V/VO
0.0	0.0	42.09247	1.000
2.4	0.1	42.09247	1.000
4.8	0.2	42.09247	1.000
7.3	0.3	41.43857	0.984
9.7	0.4	35.40015	0.841
12.1	0.5	25.53038	0.607
14.5	0.6	15.54395	0.369
16.9	0.7	7.98950	0.190
19.4	0.8	3.46679	0.082

***** VELOCITY IN REGION I ******

BOTTOM VELOCITY	SHEAR STRESS	SHEAR VELOCITY	GRAIN SIZE
0.913E 01	0.498E 00	0.499E 00	0.503E 01

X/D= 4

R	R/D	LONGITUDINAL VELOCITY	V/VO
0.0	0.0	42.09247	1.000
2.4	0.1	42.09247	1.000
4.8	0.2	41.97714	0.997

TABLE 5.2 (CONTINUED)

7.3	0.3	39.11996	0.929
9.7	0.4	33.14467	0.787
12.1	0.5	25.53041	0.607
14.5	0.6	17.87849	0.425
16.9	0.7	11.38240	0.270
19.4	0.8	6.58818	0.157

***** VELOCITY IN REGION I ******

BOTTOM VELOCITY	SHEAR STRESS	SHEAR VELOCITY	GRAIN SIZE
0.124E 02	0.924E 00	0.681E 00	0.934E 01

X/D= 5

R	R/D	LONGITUDINAL VELOCITY	V/VO
0.0	0.0	42.09247	1.000
2.4	0.1	42.08925	1.000
4.8	0.2	40.70134	0.967
7.3	0.3	37.03130	0.880
9.7	0.4	31.69946	0.753
12.1	0.5	25.53036	0.607
14.5	0.6	19.34575	0.460
16.9	0.7	13.79230	0.328
19.4	0.8	9.25148	0.220

***** VELOCITY IN REGION I ******

BOTTOM VELOCITY	SHEAR STRESS	SHEAR VELOCITY	GRAIN SIZE
0.147E 02	0.130E 01	0.806E 00	0.131E 02

TABLE 5.2 (CONTINUED)

X/D= 6

R	R/D	LONGITUDINAL VELOCITY	V/VO
0.0	0.0	42.09247	1.000
2.4	0.1	41.43857	0.984
4.8	0.2	39.11998	0.929
7.3	0.3	35.40016	0.841
9.7	0.4	30.70612	0.729
12.1	0.5	25.53036	0.607
14.5	0.6	20.34709	0.483
16.9	0.7	15.54398	0.369
19.4	0.8	11.38240	0.270

***** VELOCITY IN REGION I ******

BOTTOM VELOCITY	SHEAR STRESS	SHEAR VELOCITY	GRAIN SIZE
0.164E 02	0.160E 01	0.896E 00	0.162E 02

X/D= 7

R	R/D	LONGITUDINAL VELOCITY	V/VO
0.0	0.0	37.11858	0.882
2.4	0.1	36.54575	0.868
4.8	0.2	34.87976	0.829
7.3	0.3	32.27019	0.767
9.7	0.4	29.94145	0.688
12.1	0.5	25.16116	0.598
14.5	0.6	21.20468	0.504
16.9	0.7	17.32307	0.412
19.4	0.8	13.71857	0.326

TABLE 5.2 (CONTINUED)

***** VELOCITY IN REGION II *****

BOTTOM VELOCITY	SHEAR STRESS	SHEAR VELOCITY	GRAIN SIZE
0.180E 02	0.194E 01	0.985E 00	0.196E 02

X/D= 8

R	R/D	LONGITUDINAL VELOCITY	V/VO
0.0	0.0	32.47874	0.772
2.4	0.1	32.09430	0.762
4.8	0.2	30.96905	0.736
7.3	0.3	29.17810	0.693
9.7	0.4	26.84464	0.638
12.1	0.5	24.11655	0.573
14.5	0.6	21.15585	0.503
16.9	0.7	18.12187	0.431
19.4	0.8	15.15769	0.360

***** VELOCITY IN REGION II *****

BOTTOM VELOCITY	SHEAR STRESS	SHEAR VELOCITY	GRAIN SIZE
0.187E 02	0.208E 01	0.102E 01	0.210E 02

X/D= 9

R	R/D	LONGITUDINAL VELOCITY	V/VO
0.0	0.0	28.87000	0.686
2.4	0.1	28.59966	0.679

TABLE 5.2 (CONTINUED)

4.8	0.2	27.80371	0.661
7.3	0.3	26.52606	0.630
9.7	0.4	24.83537	0.590
12.1	0.5	22.81898	0.542
14.5	0.6	20.57550	0.489
16.9	0.7	18.20676	0.433
19.4	0.8	15.81039	0.376

***** VELOCITY IN REGION II *****

BOTTOM VELOCITY	SHEAR STRESS	SHEAR VELOCITY	GRAIN SIZE
0.186E 02	0.207E 01	0.102E 01	0.210E 02

X/D= 10

R	R/D	LONGITUDINAL VELOCITY	V/V0
0.0	0.0	25.98300	0.617
2.4	0.1	25.78574	0.613
4.8	0.2	25.20290	0.599
7.3	0.3	24.26064	0.576
9.7	0.4	23.00035	0.546
12.1	0.5	21.47571	0.510
14.5	0.6	19.74883	0.469
16.9	0.7	17.88609	0.425
19.4	0.8	15.95405	0.379

***** VELOCITY IN REGION II *****

BOTTOM VELOCITY	SHEAR STRESS	SHEAR VELOCITY	GRAIN SIZE
0.182E 02	0.198E 01	0.997E 00	0.200E 02

Table 5.3 Summary of Computer Output for the TEXAS CALIFORNIA

Location	Bottom Velocity (ft/sec)	Grain Size for Motion (ft)
D	0.218	0.062
2D	4.43	1.18
3D	9.13	5.03
4D	12.4	9.34
5D	14.7	13.1
6D	16.4	16.2
7D	18.0	19.6
8D	18.7	21.2
9D	18.6	21.2
10D	18.2	20.0

It should be mentioned that the grain diameter in the Shields diagram was taken as the median sieve size for which 50 percent of the weight of the material was finer or coarser. Shields' diagram did not apply in this case because the sands of the bed and the bed-load, respectively, were different in size and in texture. In the case of non-uniform mixtures, Egizaroff (15) proposed an equation for incipient motion as follows:

$$\frac{\tau_o}{(r_s - r)d} = \frac{0.1}{[\log 19\ (d/\bar{d})^2]} \qquad (5.3)$$

where $\bar{d}$ = average diameter of grain for both the gradation curve for grains in movement, and for total sediment.

Case Studies

Data were collected for different ships in the Corpus Christi ship channel as shown in Table 5.4 (16). These data were used to determine incipient sediment motion in the channel. The Corpus Christi channel has a depth of 45 feet at this location.

For each ship, the maximum bottom velocity occurred at a different depth. Table 5.3 showed that the maximum bottom velocity of the TEXAS CALIFORNIA is at x = 8 D, (or x = to eight propeller diameters).

The maximum bottom velocity for the OCEAN CHEMIST, induced by the propeller, was located at x = 10 D. The critical grain size increases along the x-direction. The zone of flow establishment was reached at x = 6 D. The maximum value of R/D, vertical distance measured from the axis of the propeller/diameter of propeller (Fig. 3.1), is 1.1.

Calculated results show that the bottom velocity induced by the propeller occurred at x = 8 D for TEXAS CALIFORNIA. The TEXAS CALIFORNIA, with a draft of 37.3 ft, shows a value of R/D = 0.8 while the OCEAN CHEMIST, with a draft of 31.5 has a value of R/D = 1.1. The results for the EAGLE LEADER, which has a draft of 36.5 feet and a speed of 16 knots, were similar to those for the TEXAS CALIFORNIA, since the maximum value of R/D is equal to 0.8 in both cases.

For the EXXON NEW ORLEANS the maximum velocity induced by the propeller was at x = D. The critical grain size became large due to a deep draft of 42 feet and considerable erosion of the channel bottom could be expected. The maximum value of R/D is only 0.6.

OLANDA is a small barge of only 4,400 tons; it has a draft of only 11 feet. The results show that the bottom velocity could be neglected and little sediment motion can be expected. The maximum value of R/D is

Table 5.4 Ship Records from Corpus Christi Channel (from ref. 16)

SHIP NAME	TONNAGE (Dead wt tons)	DRAFT (ft)	SPEED (Knots)	ESTIMATED DIAMETER OF PROPELLER (ft)
Ocean Chemist	20,500	31.5	15.5	20.5
Texas California	42,067	37.3	18.0	24.2
Eagle Leader	37,807	36.5	16.0	23.7
Exxon New Orleans	71,508	42.0	16.5	27.3
Olanda	4,400	11.0	13.0	7.2
Post Challenger	24,900	32.5	15.25	21.2
Christine Bolton	5,613	21.9	16.0	14.2

3.0. For the POST CHALLENGER the maximum bottom velocity occurred at x = 10 D and the maximum value of R/D is 1.0.

Finally the CHRISTINE BOLTON was studied; her draft was 21.9 feet. The data showed no sediment movement from x = D to x = 3 D. The maximum value of R/D is 2.1 and the maximum bottom velocity is at x = 10 D. Table 5.5 is a summary of the maximum bottom velocity for different ships.

Table 5.5 Maximum Bottom Velocities

Ship Name	Draft (ft)	Draft/Depth	Location of Max. Bottom Velocity	Max. Bottom Velocity (ft/sec)
Ocean Chemist	31.5	0.7	10 D	10.3
Texas California	37.3	0.83	8 D	18.7
Eagle Leader	36.5	0.81	9 D	17.2
Exxon New Orleans	42.0	0.93	1 D	32.3
Olanda	11.0	0.24	10 D	0
Post Challenger	32.5	0.72	10 D	11.7
Christine Bolton	21.9	0.49	10 D	1.1

The results of the critical grain size of motion for different ships are plotted in Figs. 5.11 to 5.17. Figs. 5.11, 5.16 and 5.17 indicate that the critical grain size of motion increases with distance downstream of the propeller from x = D to x = 10 D. Fig. 5.12 shows that the critical grain size of motion increases from x = D to x = 8 D, and then decreases. Similarly, Fig. 5.13 has a maximum critical grain size at x = 9 D. Fig. 5.14 indicates that the maximum grain size is at x = 1 D.

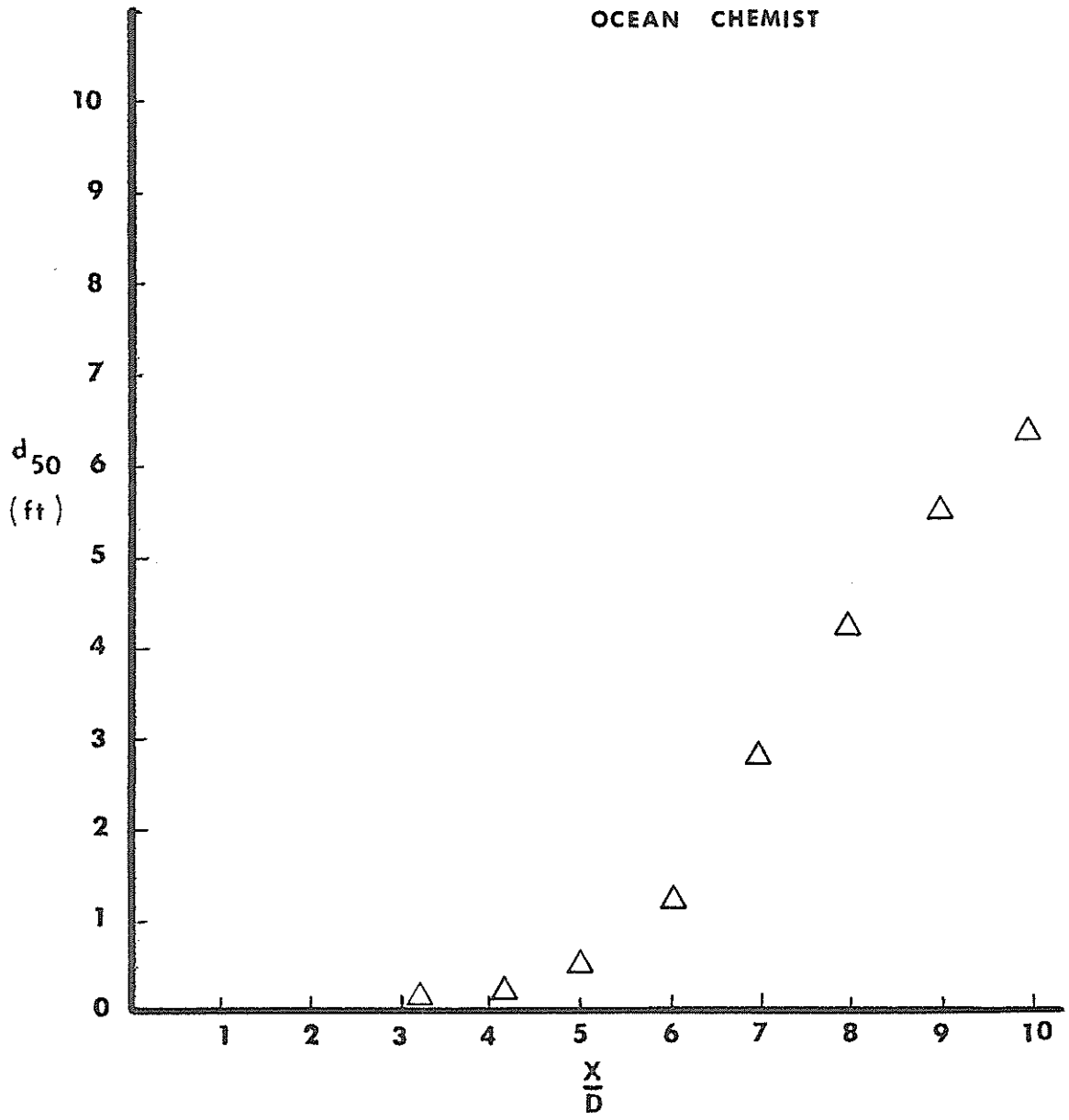

Fig. 5.11 Critical Grain Size as a Function of Relative Distance for the OCEAN CHEMIST

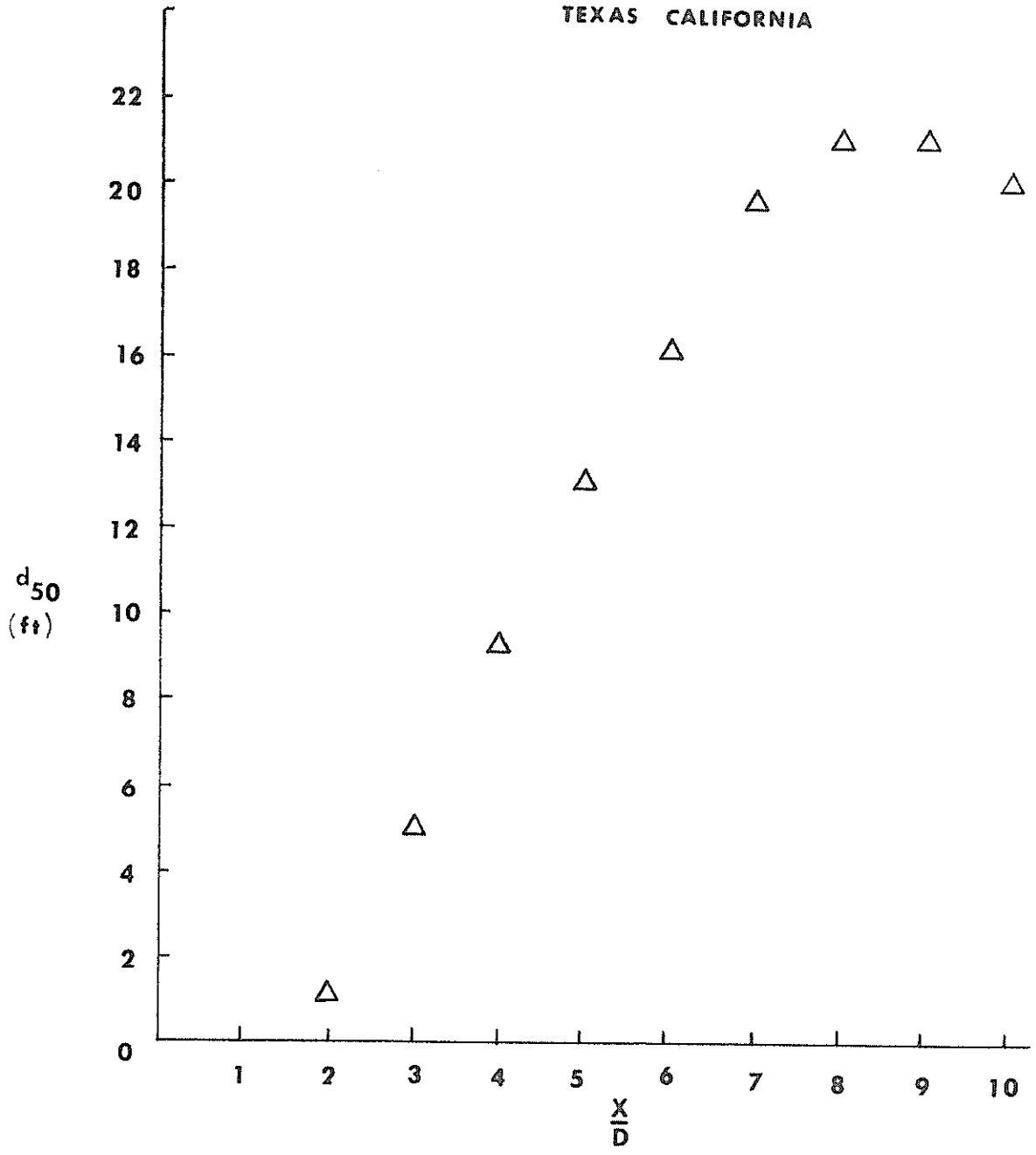

Fig. 5.12 Critical Grain Size as a Function of Relative Distance for the TEXAS CALIFORNIA

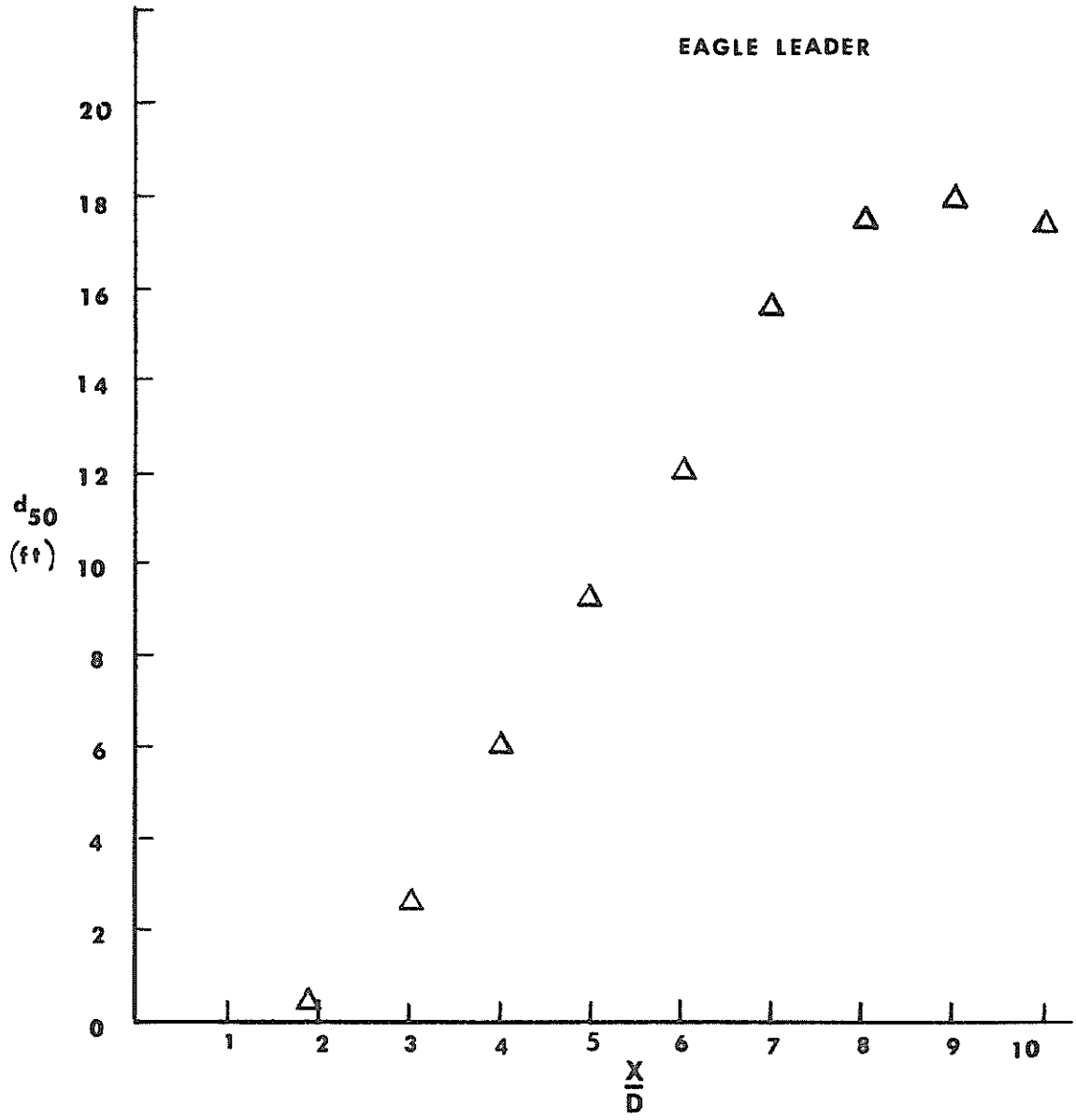

Fig. 5.13 Critical Grain Size as a Function of Relative Distance for the EAGLE LEADER

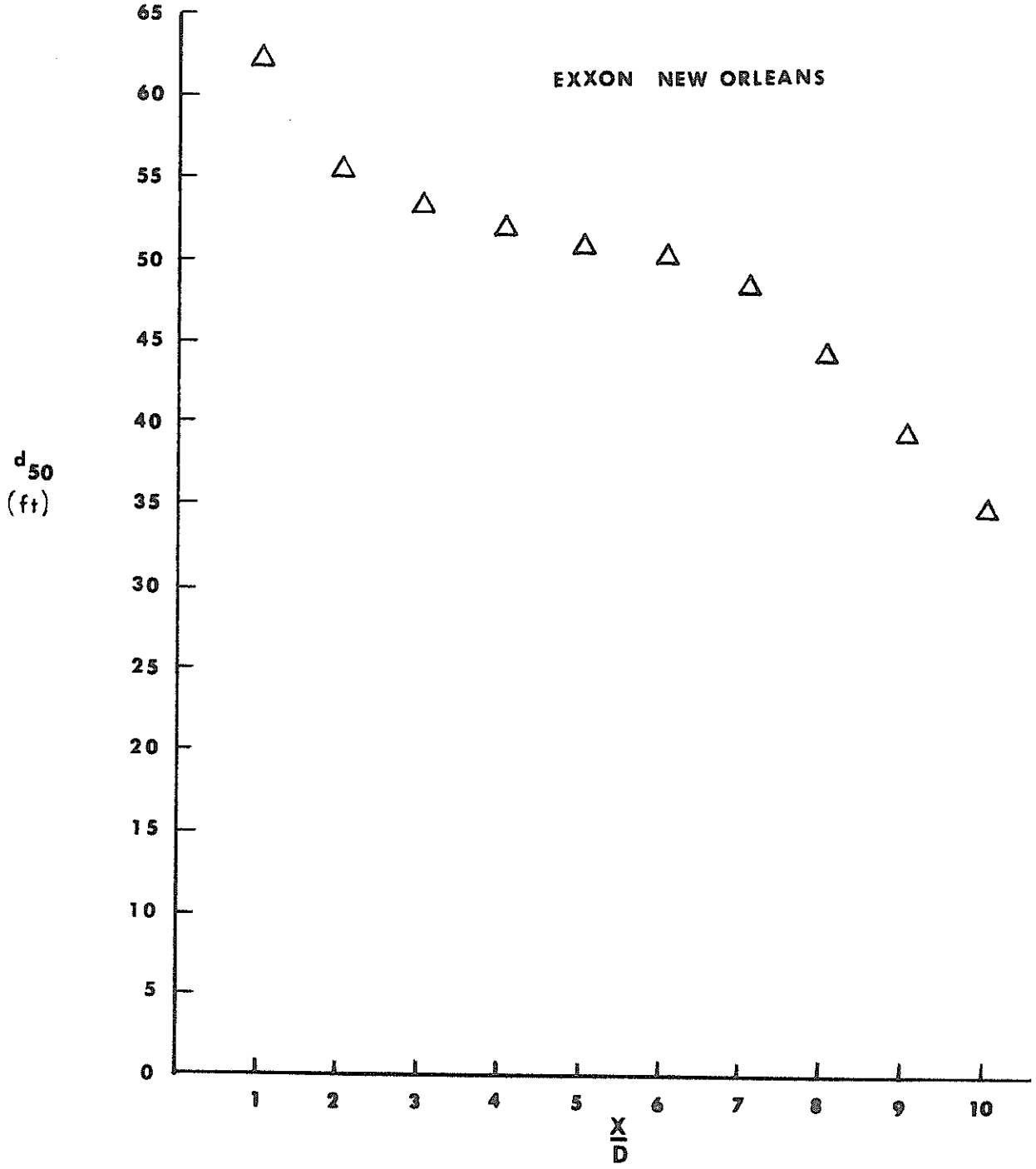

Fig. 5.14 Critical Grain Size as a Function of Relative Distance for the EXXON NEW ORLEANS

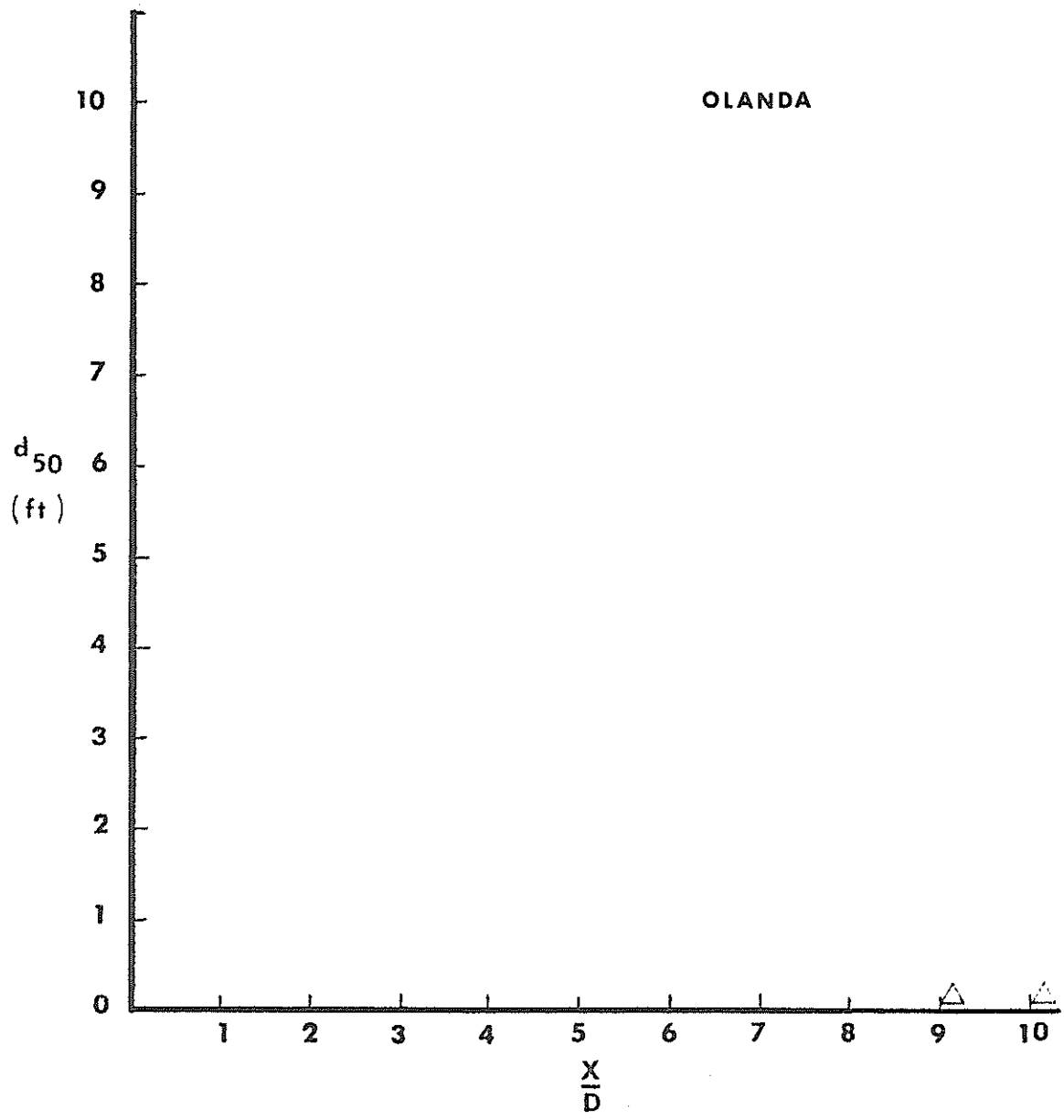

Fig. 5.15 Critical Grain Size as a Function of Relative Distance for the OLONDA

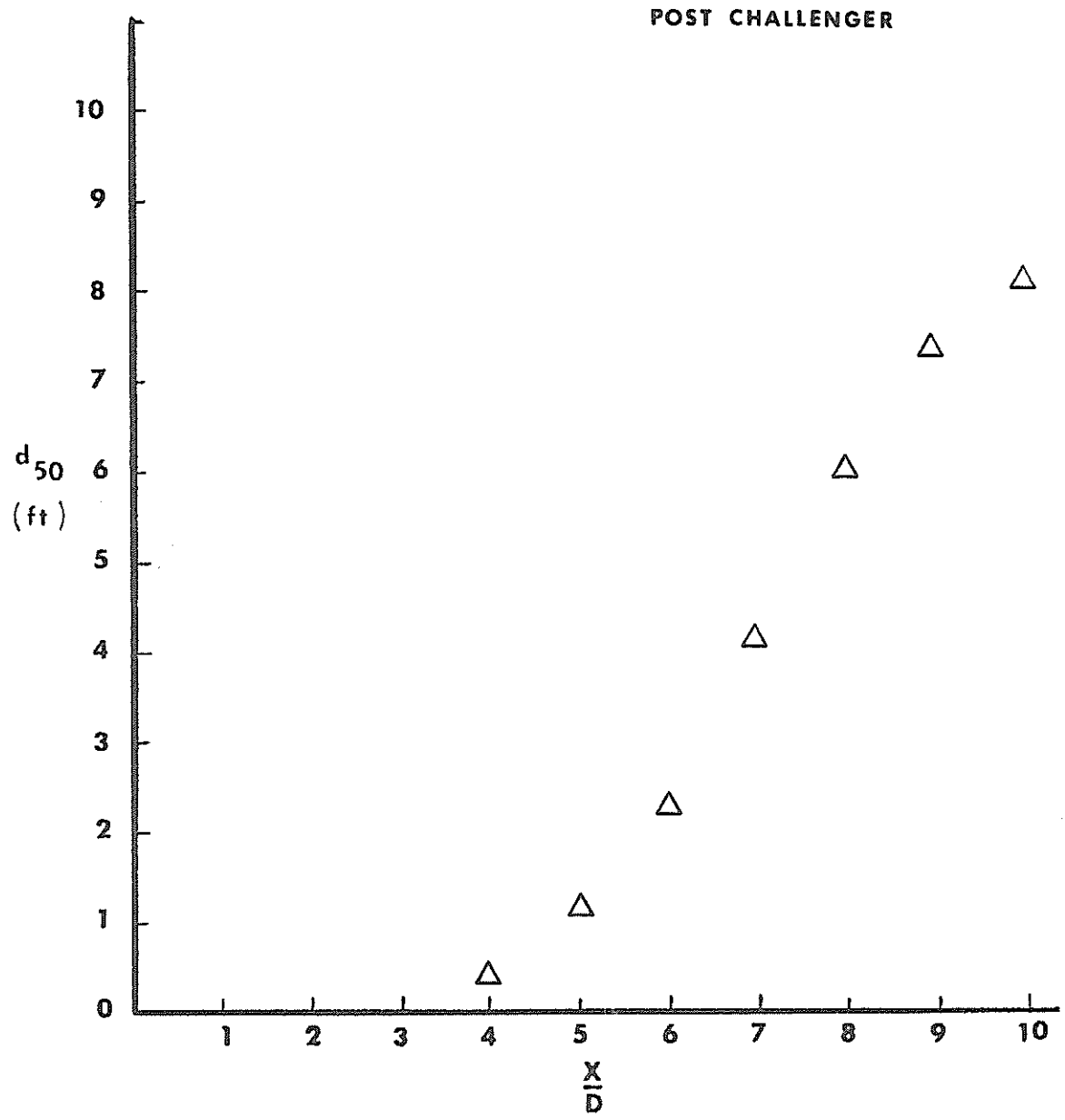

Fig. 5.16 Critical Grain Size as a Function of Relative Distance for the POST CHALLENGER

CHAPTER VI

CONCLUSIONS AND RECOMMENDATIONS

The objective of this research was to develop a numerical model capable of determining velocity distribution and initial motion of sediment induced by ships' propellers in a restricted waterway. The methods proposed are based on the momentum theory of the propeller, Gaussian normal distribution of velocity, and Shields' diagram for sediment motion.

Results obtained show that most of the sediment particles will be moved by the turbulence induced by ships' propellers. Conclusions, based on seven case studies, are as follows:

1) The velocity distribution downstream of the propeller varied with location.
2) For deep-draft vessels, the critical grain size of initial motion is more significant near the propeller than some distance downstream from it.
3) The draft of the ship is the predominant factor affecting the magnitude of sediment motion induced by the ship's propellers in the restricted waterway.

Experimental studies of turbulent motion produced should be carried out to provide additional information. Velocity distribution downstream of the propeller should be measured to provide a better understanding of the sediment motion induced by ships' propellers. An effort directed toward the description of the velocity distribution and shear stress at the boundary is recommended.

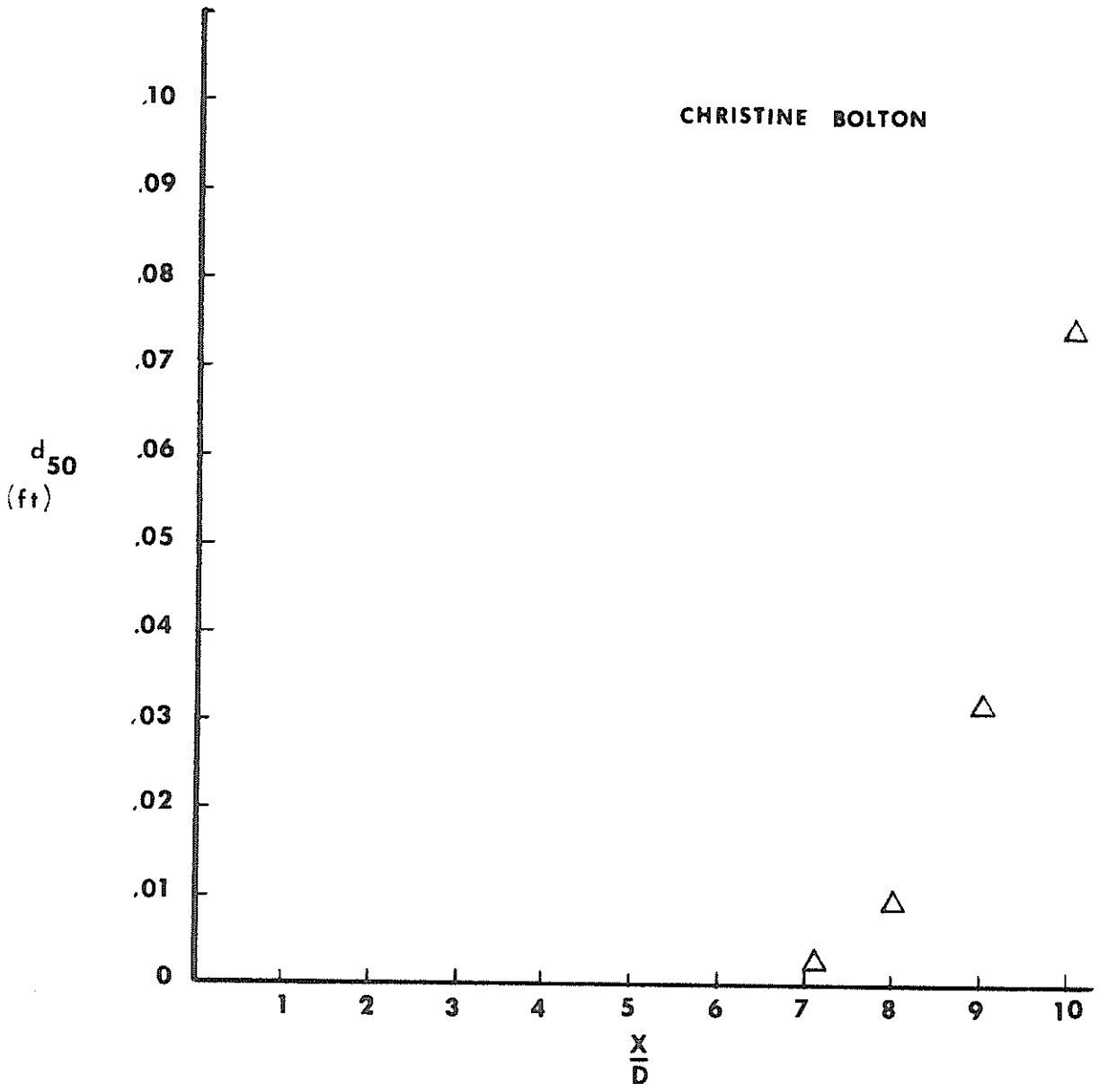

Fig. 5.17 Critical Grain Size as a Function of Relative Distance for the CHRISTINE BOLTON

These results indicate that the location of the maximum critical grain size depends on the draft of the ship. In the case of deep draft the maximum critical grain size occurs near the propeller. For the shallow draft the maximum grain size is around x = 10 D. The results also indicate that the critical grain size is around x = 10 D, and that it is very large for most ships, or that most of the particles will be moved by the ships' propellers.

From these case studies, it was found that the draft of the ship is the predominant factor affecting the sediment movement induced by the propeller in a restricted waterway. In the case of deep draft, for 0.8 < R/D < 1.0, the maximum bottom velocity occurs near the propeller. For shallow draft, R/D > 2, very little, or no sediment movement occurs.

REFERENCES

1. Abramovich, G.N., "The Theory of Turbulent Jets", The M.I.T. Press, M.I.T. Cambridge, Massachusetts, 1963.

2. Aksoy, S., "The Influence of the Relative Depth on Threshold of Grain Motion", International Symposium on River Mechanics, IAHR, Bangkok, Thailand, January 1973, pp. 359-370.

3. Albertson, M.L., Dai, Y.B., Jensen, R.A., and Rouse, H., "Diffusion of Submerged Jets", Trans., ASCE, Vol. 115, 1950, pp. 639-697.

4. Ammar, A.A., et al., "Design of Navigation Canal Cross-Section and Alignment", International Navigation Congress, Paris, 1969, pp. 191-202.

5. Apmann, R.P., Rumer, R.R., "Diffusion of Sediment in a Non-uniform Flow Field", Civil Engineering Report No. 16, University of New York, December 1967.

6. Bagnold, R.A., "An Approach to the Sediment Transport Problem from General Physics", Geological Survey Professional Paper 422-I, United States Government Printing Office, Washington, 1966.

7. Balanin, V.V., Bykov, L.S., "Selection of Leading Dimensions of Navigations of Navigation Canal Section and Modern Methods of Bank Protection", International Navigation Congress, Section I-4, Stockholm, 1965, pp. 151-169.

8. Bogardi, J.L., "European Concepts of Sediment Transportation", Journal of the Hydraulics Division, ASCE, Vol. 91, No. HY1, January 1965, pp. 29-54.

9. Brooks, N.H., "Calculation of Suspended Load Discharge from Velocity and Concentration Parameters", Miscellaneous Publication 970, U.S. Department of Agriculture, 1963, pp. 229-237.

10. Carstens, T., Rao, U.M., "Sediment-Laden Submerged Horizontal Jets", IAHR, France, 1971, pp. 135-144.

11. Chien, M., "The Present Status of Research on Sediment Transport", Trans., ASCE, Vol. 121, 1956, pp. 833-884.

12. Comstock, J.P., "Principles of Naval Architecture", The Society of Naval Architecture and Marine Engineers, New York, N.Y., 1967.

13. Einstein, H.A., "The Bed-Load Function for Sediment Transportation in Open Channel Flows", U.S. Dept. of Agriculture, Technical Bulletin No. 1926, 1950.

14. Garrelts, I.E., "Problem Arising From the Use of Very Large Ships in Connection with the Alignment and Depth of Approach Channels and of Maneuvering Areas", International Navigation Congress, Section II-3, Paris, 1969, pp. 5-30.

15. Graf, W.H., "Hydraulics of Sediment Transport", McGraw-Hill Book Company, N.Y., 1971.

16. Herbich, J.B., Personal Communication, 1975.

17. Hjelemfelt, A.T., Lenau, C.W., "Effect of Concentration of Sediment Distribution", Journal of the Hydraulics Division, ASCE, Vol. 91, No. HY5, 1965, pp. 1775-1779.

18. Ippen, A.T., "The Interaction of Velocity Distribution and Suspended Load in Turbulent Streams", International Symposium on River Mechanics, IAHR, Bangkok, Thailand, January 1973, pp. 341-369.

19. O'Brien, M.P., "Review of the Theory of Turbulent Flow and Its Relation to Sediment Transportation", Trans. Am. Geophys. Union, 1933, 34:487-491.

20. Pai, S.I., "Fluid Dynamics of Jets", D. Van Nostrand Company, Inc., 1960.

21. Rouse, H., "Advanced Mechanics of Fluids", John Wiley & Sons, Inc., New York, 1959.

22. Saunders, H.E., "Hydrodynamics in Ship Design", The Society of Naval Architects and Marine Engineers, New York, 1957.

23. Schiller, R.E., "A Study of Transport in the Indus Basin Canal", Ph.D. Dissertation, Colorado State University, Fort Collins, Colorado, December 1968.

24. Schlichting, H., "Boundary Layer Theory", McGraw-Hill Book Company, Inc., 1960.

25. Vanoni, V.A., et al., "Sediment Transportation Mechanics: Suspension of Sediment Journal of the Hydraulics Division, ASCE, Vol. 89, No. HY5, 1963, pp. 45-76.

26. Singamsetti, S.R., "Diffusion of Sediment in a Submerged Jet", Journal of the Hydraulics Division, ASCE, Vol. 92, No. HY2, 1966, pp. 153-168.

27. Shen, H.S., "River Mechanics", Dept. of Civil Engineering, Colorado State University, Vol. I, 1971.

28. Sternberg, R.W., "Predicting Initial Motion and Bedload Transport of Sediment Particles in the Shallow Marine Environment", Shelf Sediment Transport, Dowden Hutchinson & Ross, 1972.

29. Sutherland, A.T., "Entrainment of Fine Sediments by Turbulent Flows", Report No. KH-R-13, California Institute of Technology, June 1966.

30. Vanoni, V.A., "Measurements of Critical Shear Stress for Entraining Fine Sediments in a Boundary Layer", California Institute of Technology, Report No. KH-R-7, May 1964.

31. Vanoni, V.A., "Transportation of Suspended Sediment by Waters", Trans., ASCE, Vol. III, pp. 67-133.

32. White, C.M., "The Equilibrium of Grain in the Bed of a Stream", Proc. Royal Society A., Vol. 174, 1940, pp. 324-338.

33. Wiegel, R.L., "Oceanographical Engineering", Prentice-Hall, Inc., 1964.

34. Zagustin, K., "Sediment Distribution in Turbulent Flow" Journal of Hydraulic Research, IAHR, Vol. 6, No. 2, 1968, pp. 163-172.